VNIVERSITAT DE VALÈNCIA Facultat de Física

Màster en Física Avançada

Especialitat Física Teòrica

Treball Fi de Màster

Neutrino Masses, Dark Matter and the Baryon Asymmetry in a low-scale seesaw model

Andreu Sanjuan Silvestre

Tutor: Juan Herrero García
Giacomo Landini

Curs acadèmic 2024/25

Contents

Abstract

The seesaw mechanism is one of the most well-motivated extensions of the Standard Model, as it provides an elegant explanation for neutrino masses through the introduction of three heavy Majorana right-handed neutrinos. When combined with leptogenesis, it can also account for the baryon asymmetry of the universe (BAU). However, it does not explain the nature of dark matter (DM) on its own. In this work, building on the model proposed by Juan Herrero García, Giacomo Landini, and Tsutomu T. Yanagida [1], we propose a minimal extension incorporating a dark sector consisting of a Majorana singlet fermion (as the DM candidate) and a complex scalar singlet. In this framework, right-handed neutrinos generate the cold DM abundance through their decays. Additionally, interactions between the dark sector and the Standard Model predict an extra dark component arising from Higgs-portal couplings between the scalar and the Higgs boson. A further subdominant DM component can also emerge from late-time scalar decays, accompanied by an additional population of active neutrinos. The resulting electromagnetic energy injection leaves observable imprints on cosmological probes such as Big Bang Nucleosynthesis (BBN) and the Cosmic Microwave Background (CMB). In this context, the constraints on the parameter space allow for an analysis in the regime of low right-handed neutrino masses.

1 Introduction

The Standard Model of particle physics (SM) represents the most complete and thoroughly tested physical theory to date. This universal framework describes both the fundamental constituents of matter, such as quarks and leptons, and the bosons that mediate the four fundamental forces of the universe, including the Higgs boson. In this way, the SM provides an understanding of the physical principles governing the universe, offering a representation of the various interactions among fundamental particles within a $SU(3)_C \times SU(2)_L \times U(1)_Y$ gauge symmetry group. However, despite the significant successes of this theory, it fails to account for many of the unresolved mysteries of our universe. A key element in understanding this work is the role of neutrinos, which belong to the lepton family.

Firstly introduced by Wolfgang Pauli in 1930 [2], neutrinos are electrically neutral, spin fermions which only interact through the weak force and gravity. Pauli postulated the existence of these new particles in order to account for the missing energy and momentum in beta decay. The experimental discovery by Cowan and Reines in 1956 confirmed the existence of neutrinos [3] and the conservation of angular momentum in decays. The SM remains, to this day, the most successful and precise description of the known fundamental particles and their interactions. It accurately predicts a wide range of phenomena and has withstood extensive experimental scrutiny. With the discovery of the Higgs boson in 2012, the model was thought completed, validating the mechanism of electroweak symmetry breaking and mass generation for the charged fermions and gauge bosons.

However, despite its triumphs, the SM is incomplete. It does not provide a mechanism to generate non-zero neutrino masses, which are now firmly established by multiple experiments. The assumption of massless neutrinos is no longer tenable, implying that the SM must be extended in some way to accommodate the observed properties of neutrinos [4, 5, 6, 7, 8, 9].

Moreover, the SM fails to account for one of the most fundamental features of our Universe: the baryon asymmetry of the Universe (BAU, Section 1.2). Observational data, such as the cosmic microwave background and the abundance of light elements, point to a significant matter–antimatter asymmetry, quantified by a baryon-to-photon ratio which has been measured by WMAP5 observations [10]. The main problem is that the SM does not have mechanisms to reproduce the sufficient amount of CP violation that leads to the observed asymmetry, such that new models have been introduced, among which Leptogenesis stands out as a compelling mechanism to explain the BAU, detailed in Refs. [4, 6, 8, 9, 11, 12, 13, 14, 15].

A further crucial limitation is its inability to explain the existence of dark matter, which constitutes around 27% of the energy density of the Universe. As detailed in Section 1.3, evidence from galactic rotation curves, gravitational lensing, large-scale structure formation, and the cosmic microwave background confirms the presence of a non-luminous, non-baryonic component of matter, whose properties cannot be explained in terms of SM physics.

Thus, the quest to uncover the origin of neutrino mass, alongside the need to account for the BAU and to explain both the origin and composition of dark matter, leads us to explore theories beyond the Standard Model (BSM) that can explain these shortcomings. This is the motivation behind the work, due to importance of developing simple, testable models capable of addressing these shortcomings in a coherent framework.

In this work, we will first discuss the main shortcomings of the Standard Model, presented in the Sections 1.1, 1.2 and 1.3. Moreover, in Section 2, it will be included the framework of this model, based on the seesaw mechanism, while Section 3 is based on the main DM production mechanisms. Section 4 is focused on Leptogenesis as a BSM theory that explains the BAU. Finally, in Section 5 it has been introduced our model, where it will be expanded the main interactions that must be taken into account to reproduce the DM abundance (see Sections 5.2, 5.3 and 5.4), as well as numerical constraints over the model introduced from observations, presented in Section 5.5. Finally, in Sections 6 and 7 we introduce the results obtained through this model, and a final discussion of the influence of these results.

1.1 Neutrino masses

In 1930, when Pauli introduced neutrinos, they were thought to be similar to neutrons with extremely small masses. Within the framework of the SM of particle physics [16], neutrinos are described as massless, purely left-handed particles, forming part of weak isospin doublets alongside their charged lepton partners. Because they carry no electric charge, neutrinos interact only through the weak and gravitational force, giving them an interaction cross-section so small that trillions traverse the Earth each second virtually unhindered. Hence, their main interactions [4] are given by:

1. Charged - Current (CC) and Neutral Current (NC) interactions: Interactions via $W^{\pm}$ or Z bosons arise from the interaction Lagrangian

$$\mathcal{L}^{SM}_{CC}(x) = -\frac{g_W}{2\sqrt{2}} j^{\mu}_W(x) W_{\mu}(x) + h.c.\,, \qquad \mathcal{L}^{SM}_{NC}(x) = -\frac{g_W}{2cos\theta_W} j^{\mu}_Z Z_{\mu}(x)\,, \tag{1.1}$$

where $g_2 \simeq 0.65$ is the $SU(2)_L$ weak coupling constant, θ_W is the weak mixing angle with $\sin^2\theta_W \simeq 0.23121$ [16]; and $W_{\mu}(x)$ and $Z_{\mu}(x)$ are the 4-component vector fields describing the $W^{\pm}$ and Z weak massive bosons. The weak currents are defined as

$$j^{\mu}_W(x) = 2 \sum_{\alpha=e,\mu,\tau} \overline{\nu_{\alpha L}} \gamma^{\mu} \alpha_L(x)\,, \tag{1.2}$$

$$j^{\mu}_Z(x) = 2 \sum_{\alpha=e,\mu,\tau} [g^{\nu}_L \overline{\nu_{\alpha L}} \gamma^{\mu} \alpha_L(x) + g^{\alpha}_L \overline{\alpha_L} \gamma^{\mu} \alpha_L(x) + g^{\alpha}_R \overline{\alpha_R} \gamma^{\mu} \alpha_R(x)]\,, \tag{1.3}$$

where $\alpha_R(x)$ represent the right-handed chiral field for the charged lepton $\alpha = \{e, \mu, \tau\}$; and the couplings take the values $g^{\nu}_L = +1/2$, $g^{\alpha}_L = -1/2 + \sin^2\theta_w$, and $g^{\alpha}_R = \sin^2\theta_w$.

2. Oscillations: Neutrinos were introduced into the SM as three flavor eigenstates ν_{α}, with $\alpha = e,\ \mu,\ \tau$, which are coherent mixtures of three distinct mass eigenstates. As a result, flavor-changing phenomena come from oscillations between neutrino flavors, which naturally emerges from the nature of their interactions in the SM. This arises from the fact that the structure of weak interactions is diagonal in the flavor basis, but they are not in the mass representation. When neutrinos were proposed, they were assumed to be massless, as there was no possible mass term arising from the theory.

Neutrinos were assumed to be massless until 1998, when the results from the Super-Kamiokande experiment in Japan announced [17] the first conclusive evidence of neutrino oscillations, direct proof of non-zero neutrino masses. Specifically, they observed that muon neutrinos were changing flavor during propagation, implying that at least two neutrinos have non-zero masses.

It has been widely established by experiments investigating solar, atmospheric, reactor, and accelerator neutrinos that neutrinos undergo flavor oscillations: a neutrino, being initially in a flavor eigenstate ν_α (antineutrino $\overline{\nu_\alpha}$), after propagating a certain distance for a period of time t, can be detected as a neutrino of a different flavor ν_β (antineutrino $\overline{\nu_\beta}$), $\beta \neq \alpha$, with a non-zero probability $P(\nu_\alpha \to \nu_\beta, t) \neq 0$. As stated in [16], the neutrino mixing scheme explains the origin of these oscillations by assuming that neutrinos are composed of a mixture of the three lepton flavor states, $\nu_{\alpha L} = \sum_a \mathcal{U}_{\alpha a}\nu_{aL}$, where ν_{aL} represents a neutrino mass eigenstate with mass m_a, and $\mathcal{U}$ is the 3×3 unitary Pontecorvo-Maki-Nakagawa-Sakata (PMNS) neutrino mixing matrix ([18, 19, 20]). By adopting the standard parametrisation, the PMNS matrix can be written as [4, 21]

$$U = \begin{pmatrix} c_{12}c_{13} & s_{12}c_{13} & s_{13}e^{-i\delta} \\ -s_{12}c_{23} - c_{12}s_{23}s_{13}e^{i\delta} & c_{12}c_{23} - s_{12}s_{23}s_{13}e^{i\delta} & s_{23}c_{13} \\ s_{12}s_{23} - c_{12}c_{23}s_{13}e^{i\delta} & -c_{12}s_{23} - s_{12}c_{23}s_{13}e^{i\delta} & c_{23}c_{13} \end{pmatrix} \times \begin{pmatrix} 1 & 0 & 0 \\ 0 & e^{i\frac{\alpha_{21}}{2}} & 0 \\ 0 & 0 & e^{i\frac{\alpha_{31}}{2}} \end{pmatrix}, \tag{1.4}$$

with $c_{ab} \equiv \cos\theta_{ab}$, $s_{ab} \equiv \sin\theta_{ab}$, where $\theta_{ab} \in [0, \pi/2]$ represent the mixing angles, $\delta \in [0, 2\pi]$ is the Dirac phase; α_{21} and $\alpha_{31} \in [0, 2\pi]$ are the Majorana phases. As a flavor state $|\nu_\alpha\rangle = \sum_a \mathcal{U}^*_{\alpha a}|\nu_a(t)\rangle$ is a coherent superposition of massive states, under the plane-wave approximation one can study the evolution of the probability of the oscillation as

$$P(\nu_\alpha \to \nu_\beta, t) = |\langle\nu_\beta|\nu_\alpha(t)\rangle|^2 \simeq \left| \sum_a \mathcal{U}^*_{\alpha a}\mathcal{U}_{\beta a} \exp\left(-i\frac{\Delta m^2_{ab} L}{2E_\nu} \right) \right|^2, \tag{1.5}$$

where $\Delta m^2_{ab} = m^2_a - m^2_b$, and $L \simeq ct$ is the distance travelled by the initial relativistic neutrino with energy $E_\nu \simeq p_\nu$, being p_ν its momentum. Using data from oscillations of solar and atmospheric neutrinos, as well as from those produced in accelerators, the mixing parameters and squared mass differences can be inferred. For instance, the most recent NuFit 5.2 global analysis [22, 23, 24] reported the following best-fit $\pm 1\sigma$ values and 3σ ranges of the mixing parameters in the case of a neutrino mass spectrum with normal (inverted) ordering, the values are:

$$\theta_{12} = 33.41^{+0.75}_{-0.71}, \quad \theta_{13} = 8.58 \ \pm \ 0.11, \quad \theta_{23} = 42.2^{+1.1}_{-0.9}$$
$$\Delta m^2_\odot/(10^{-5}\text{eV}^2) = 7.41^{+0.21}_{-0.20}$$
$$\Delta m^2_{\text{atm}}/(10^{-5}\text{eV}^2) = 2.507^{+0.026}_{-0.027}$$

where $\Delta m^2_\odot \equiv \Delta m^2_{21}$, while the definition of Δm^2_{atm} depends on the ordering:

- Normal ordering (NO): $m_1 < m_2 < m_3$, $\Delta m^2_{\text{atm}} \equiv \Delta m^2_{31} > 0$;
- Inverted ordering (IO): $m_3 < m_1 < m_2$, $\Delta m^2_{\text{atm}} \equiv \Delta m^2_{32} < 0$.

The discovery of neutrino oscillations leads to the conclusion that at least two of the neutrinos are massive, hence new physics beyond the SM is needed in order to explain the origin of these masses (Section 2).

1.2 The Baryon Asymmetry of the Universe

So far, no traces of cosmological antimatter have been observed. The presence of a small amount of antiprotons and positrons in cosmic rays can be consistently explained by their secondary origin in cosmic particle collisions or highly energetic astrophysical processes, but no

antinuclei, even as light as anti-deuterium or as tightly bounded as anti-α particles, have ever been detected.

These observations indicate that the number of baryons (protons and neutrons) in the Universe are unequal to the number of anti-baryons (antiprotons and antineutrons). Since various considerations suggest that the Universe has started from a state with equal numbers of baryons and antibaryons, the observed baryon asymmetry must have been generated dynamically, a scenario known as Baryogenesis, proposed in 1967 by Andrei D. Sakharov [25] (for more detail see Ref. [6, 14, 15, 26, 27]).

One may wonder why it is thought that the baryon asymmetry has been dynamically generated, rather than being an initial condition. There are at least two reasons for that. On the one hand, if a baryon asymmetry had been an initial condition, it would have been a highly fine-tuned one, a condition which seems very implausible. On the other hand, and perhaps more importantly, based on observed features of the cosmic microwave background radiation, it is completely reasonable to think that inflation took place during the early history of the Universe [28, 29, 30]. Hence, any primordial baryon asymmetry would have been exponentially diluted away by inflation.

The SM contains all the ingredients that are necessary to dynamically generate such an asymmetry in an initially baryon-symmetric Universe. However, it is unable to reproduce a large value of the observed asymmetry, thus requiring the introduction of new physics. An extension of the SM must distinguish matter from antimatter in a more pronounced way than the weak interactions do. The baryon asymmetry of the Universe can be defined as [6]

$$\eta \equiv \left.\frac{n_B - n_{\bar{B}}}{n_\gamma}\right|_0 = (6.21 \pm 0.16) \times 10^{-10}\,, \tag{1.6}$$

$$Y_{\Delta B} \equiv \left.\frac{n_B - n_{\bar{B}}}{s}\right|_0 = (8.75 \pm 0.23) \times 10^{-11}\,, \tag{1.7}$$

where $n_B \approx 3.54 \times 10^{-7}$ cm^{-3} is the number density of baryons, $n_{\bar{B}}$ that of anti-baryons, $n_\gamma = (410.7 \pm 0.5)$ cm^{-3} the photon number density and $s = (2890 \pm 10)$ cm^{-3} the entropy density of the Universe, values inferred from Planck results [31] .

On the other hand, we can relate the baryon density to the baryonic fraction of the critical energy density, $\Omega_B \equiv \rho_B/\rho_{\rm crit}$, as

$$\eta = 2.74 \times 10^{-8}\ \Omega_B\, h^2\,, \tag{1.8}$$

where $h \equiv H_0/(100$ km s^{-1} Mpc$^{-1})$ is the reduced Hubble parameter at the present time, where $H_0 = (67.27 \pm 0.60)$ km s^{-1} Mpc^{-1} (68% C.L.) was obtained from Planck observations [31] The value of the baryon asymmetry of the Universe is inferred from observations in two independent ways. On the one hand, the value is obtained using data from Big Bang Nucleosynthesis (BBN), by confronting the abundances of the light elements such as D (deuterium), ^{3}He, ^{4}He, and ^{7}Li, with its theoretical predictions. In particular, the estimations of the abundances of D and ^{3}He are very sensitive to the abundance of baryons, parametrized by η. This can be understood from the fact that those light elements are crucial in the synthesis of ^{4}He via two body reactions

$$\begin{aligned} {}^3\mathrm{He} + \mathrm{D} &\to {}^4\mathrm{He} + \mathrm{p}\,, \\ {}^3\mathrm{H} + \mathrm{D} &\to {}^4\mathrm{He} + \mathrm{n}\,, \\ {}^3\mathrm{He} + {}^3\mathrm{H} &\to {}^4\mathrm{He} + \mathrm{p} + \mathrm{n}\,, \end{aligned}$$

whose interaction rates are proportional to the number densities of the incoming nuclei, which depend on η. Finally, the primordial abundances of the four light elements can be inferred from various observations, leading to a range for the baryon asymmetry given (at 95% CL) by [32]

$$4.7 \times 10^{-10} \le \eta \le 6.5 \times 10^{-10}\,, \quad 0.017 \le \Omega_B h^2 \le 0.024\,. \tag{1.9}$$

On the other hand, Ω_B can be determined from measurements of the cosmic microwave background (CMB) anisotropies. The CMB spectrum corresponds to an excellent approximation to blackbody radiation with a nearly constant temperature T. The main observable in the CMB spectrum is the temperature fluctuation in a given direction $\hat{n}$, $\Theta(\hat{n}) = \Delta T/T$. Before the time of recombination, at redshift $z_{\rm rec} \sim 1000$, the cosmological plasma can be described as a photon-baryon fluid. The main features of the CMB follow from the basic equations of fluid mechanics, which are given by

$$\ddot{\Theta} + c_s^2 k^2 \Theta = F\,, \tag{1.10}$$

where $c_s = 1/\sqrt{3(1+3\rho_B/\rho_\gamma)}$ is the sound speed in the fluid, k represents the wavenumber in Fourier space. F manifests the outcomes produced due to gravitational modifications and baryon impacts, which arise from the baryon energy density ρ_B. The physical effect of the baryons is to provide extra gravity which enhances the compression into potential wells leading to an enhancement of the compressional phases. This compression of the phases affects to the CMB spectrum, producing an enhancement of the odd peaks. Thus, a measurement of the odd/even peak disparity constraints the baryon energy density. From the most recent observations of WMAP5 [33], one gets

$$0.02149 \leq \Omega_B h^2 \leq 0.02397\,, \tag{1.11}$$

value in complete consistency with the value from the BBN observations in Eq. 1.9. Up to this point, it is known that the fact that the Universe is created by matter and not by antimatter is due to this baryon asymmetry produced in the early Universe. Nevertheless, this asymmetry was not initially present in the early Universe, but was dynamically generated during the expansion due to certain processes. The three necessary conditions to dynamically generate a baryon asymmetry in the early Universe were established in 1967 by Andrei D. Sakharov in Ref. [25]:

1. Baryon number violation: in order to evolve from an initial scenario with no baryon asymmetry $Y_{\Delta B} = 0$ to a final asymmetric state with $Y_{\Delta B} \neq 0$, it is necessary to introduce processes which violate baryon number.

2. C and CP violation: if either C or CP were conserved, any physical process involving baryons would proceed at precisely the same rate as its C- or CP- conjugate process, involving antibaryons, with the overall effect that no baryon asymmetry is generated.

3. Out-of-equilibrium dynamics: The equilibrium distribution functions n_{eq} are determined by the particle energy E, the chemical potential μ, and by its mass. Because of the CPT theorem, the mass is the same for particles and antiparticles. Under these conditions, the asymmetry of a particle P can be given in terms of the chemical potential as $A_P = \mu_P$. As long as a particle is kept in thermal equilibrium (with number-changing processes), its chemical potential vanishes $\mu_P = 0$, so that there is no asymmetry left.

The mechanism that describes the production of the baryon asymmetry is known as Baryogenesis. Despite the fact that Sakharov conditions are all satisfied in the SM, the total amount of CP violation is quantitatively too small to explain the observed value of the baryon asymmetry.

Soon after the discovery of neutrino masses, the mechanism of Leptogenesis was proposed and gained increasing popularity. This relates the BAU with neutrino physics, in particular with neutrino mass generation, via the seesaw mechanism, as will be seen in Section 2. Leptogenesis, Section 4, was first proposed by Fukugita and Yanagida in 1987 [11] in order to explain how this Baryon asymmetry arises from a Lepton one produced in the early Universe. The simplest and most theoretically well-motivated realization is precisely the Seesaw mechanism [5], where new Majorana right-handed neutrinos N_i, large masses $M_i \gg v_{\rm EW} \simeq 246$ GeV, are added to the SM particle spectrum. Usually referred to as *sterile*, they are embedded as singlets under the SM gauge interactions. The complex Yukawa coupling of these sterile neutrinos induces CP-violating decays, while the Majorana terms in the Lagrangian accounting for their masses, imply that the lepton number is not conserved. Hence, a lepton asymmetry can be generated dynamically, and then be converted into a baryon one among the SM sphaleron processes, first proposed in 1983

by Manton [34] as static unstable solutions of the electroweak model mediating transitions with baryon and lepton number violation [35].

1.3 Dark Matter

Throughout human history, it has been always sought to understand and explain the world around us. Already in the 20th century, physicists began to understand the structure of matter, as well as its composition and behavior on both large and small scales. However, up to day it is known that this baryon matter, which has long intrigued scientists, makes up no more than 7% of the known Universe. But what is the rest of the known Universe made of? The short answer is Dark Matter.

In the early 1930's, astronomers began studying large-scale structures of the Universe, owing to the development of more powerful telescopes and advancements in spectroscopy. In 1933, Fritz Zwicky took a particular interest in the Coma Cluster, a group of over a thousand galaxies located approximately 320 million light-years from Earth. Through his observations, he realized that the galaxies in the Cluster were moving at extremely high velocities, of the order of ~ 1000 km/s. If only the visible mass were considered, these velocities would be too high for the cluster to remain gravitationally bound. By applying the Virial theorem, which states that, for a system in gravitational equilibrium, the average kinetic energy $\langle T \rangle$ is related to the average gravitational potential energy $\langle U \rangle$ as

$$2\langle T \rangle + \langle U \rangle = 0\,, \tag{1.12}$$

Zwicky realized that the total required mass was at least 400 times the observed one. This led him to postulate the existence of a large amount of invisible matter that did not interact electromagnetically, which he called *Dunkle Materie*.

Several years later, in 1970, Vera Rubin and Kent Ford proposed the existence of this Dark Matter under an argument based on rotation curves: spiral galaxies rotate around their vertical axes, such that by measuring the Doppler shift of atomic lines one can determine the circular velocity of stars and other tracers as a function of their distance from the galactic center, resulting in what is known as a rotation curve. On the other hand, Newton's law $F = ma$ predicts a simple relation between the circular velocity v_c of a particle of mass m rotating within a distance r from the center of a system with mass $M(r)$. Assuming spherical symmetry, one obtains an expression which relates the rotational velocity of an object orbiting around a mass $M(r)$ with the distance from the center r:

$$m\frac{v_c^2}{r} = G\frac{M(r)m}{r^2} \quad \Rightarrow \quad v_c(r) = \sqrt{\frac{GM(r)}{r}}\,. \tag{1.13}$$

Under this relation, the velocity should then follow a Keplerian decline $v_c(r) \propto r^{-1/2}$. However, the observations of a large sample of such galaxies have shown that the rotation curves remain flat out to large distances from the galactic centers. Hence, additional invisible mass must be present to reproduce the actual orbits and velocities of stars. Subsequently, Vera Rubin and Kent Ford performed the first precise measurement of the rotation curve of the Andromeda galaxy (M31) [36], tracing about 70 hydrogen clouds. In this paper they showed that spiral galaxies rotate at constant speeds even far from the center, up to distances ~ 50 kpc and beyond. Finally, the results presented in 2018 from Planck telescope [37] confirmed the existence of non-baryonic Dark Matter from the CMB anisotropies, results consistent with a fraction $\sim 27\%$ of the energy density of the Universe. The current cosmological DM density is provided by the best-fit parameters [16]

$$\Omega_{DM}h^2 = 0.1200 \;\pm\; 0.0012\,, \tag{1.14}$$

where $\Omega_i = \rho_i/\rho_{crit}$, with the critical density $\rho_{crit} = 3H^2/8\pi G$. The present Hubble parameter is written as $H_0 = h \times 100$ km/s Mpc, with $h = 0.674 \;\pm\; 0.005$ [38].

Currently, there are various evidences for the existence of DM, coming from galactic rotation curves, galaxy clusters, gravitational lensing, CMB anisotropies and large-scale structure formation. Despite this, there is still no theory that explains its origin and composition. Indeed, all the evidence for DM is based on its gravitational interactions. Aside from that, it is known that DM must be electrically neutral and very weakly coupled to the SM sector to avoid current bounds. Furthermore, it must be stable on cosmological timescales in order to reproduce the present-day abundance. In addition, a very important fact is that must have been non-relativistic at the time of structure formation (Cold Dark Matter), as relativistic particles have large thermal velocities and hence free-stream across long distances. Therefore, they should smooth out small-scale fluctuations below a characteristic length scale, leading to suppression of the gravitational collapse of small-scale structures, which is necessary for the hierarchical growth of structure observed in the Universe. There is no particle in the Standard Model that simultaneously satisfies all these properties, so new physics is required.

In recent years, several experiments have been developed to detect DM signals. As detailed in [39], experiments have been categorized into three main approaches: direct detection, indirect detection, and production in high-energy colliders. When it comes to direct detection, the main experiments are XENONnT and DarkSide, both located at the Gran Sasso National Laboratory, LUX-ZEPELIN, based at the Stanford Underground Research Facility, and PandaX in China. These searches are based on the direct scattering of a DM particle on some target nuclei. On the other hand, indirect detection is based on the detection of standard particles produced by the annihilations or decays of DM in halos, such that the main target for observations is the galactic center and dwarf galaxies. The relevant detectors are Fermi-LAT; AMS-02, which is installed on the International Space Station; H.E.S.S., MAGIC and CTA, which are ground-based Cherenkov telescopes; and the IceCube Neutrino Observatory in the Amundsen-Scott South Pole Station.

These shortcomings, summarized in Sections 1.1, 1.2 and 1.3, point to the existence of new physics beyond the Standard Model (BSM). In this context, extensions involving mechanims for neutrino mass generation, dark sectors, and baryogenesis via leptogenesis provide an appealing and testable framework, particularly in low-scale seesaw models, which offer the intriguing possibility of connecting all three phenomena within a unified scenario. In the current work we are going to focus on a low-scale versión of the model proposed by Juan Herrero García, Giacomo Landini and Tsutomu T. Yanagida [1].

2 The Seesaw mechanism

As discussed in Section 1.1, measurements of fluxes of solar, atmospheric, reactor and accelerator neutrinos give clear evidences that at least two of the observed weakly interacting neutrinos (from now on *active* neutrinos) must be massive. This discovery challenges the Standard Model of particle physics, where neutrinos are assumed to be massless. To date, physicists have tried to discover physics beyond the Standard Model (BSM) in order to explain the origin and the smallness of neutrino masses. Among the various proposed BSM models, the seesaw mechanism stands out due to its simplicity and theoretical appeal.

First proposed in 1977 by P. Minkowski [5], this mechanism naturally emerges from extensions of the SM by including new particles (in the simplest setup, Majorana fermions, commonly referred to as *sterile* neutrinos), which are able to interact with the SM leptons. Through these new interactions, this theory is able to predict a possible origin for neutrino masses. Explicitly, if the new particle has a mass M, much heavier than the electroweak breaking scale v_{EW}, active neutrinos acquire a mass of the order of v_{EW}^2/M, much smaller than the charged fermion mass scale.

The central idea of this mechanism is that the observed active neutrino masses result from the suppression by the large mass scale associated with the new sterile neutrinos. In such a way, it is possible to reproduce the smallness of active neutrinos by enlarging the mass term proposed

for these new neutrinos. This framework not only accounts for tiny neutrino masses in a natural way but also offers a fertile ground for addressing other open questions in particle physics and cosmology, such as the origin of the baryon asymmetry of the Universe and the nature of dark matter. This section develops the theoretical foundation of the seesaw mechanism, its minimal realizations are presented, and its role in low-scale scenarios compatible with leptogenesis and dark matter phenomenology is set. Up to this point, different types of Seesaw model can be introduced depending on the properties of the heavy particles (for more details see Refs. [4, 6]).

2.1 The Type I seesaw mechanism: Singlet fermions

In the Type I seesaw model, two or three singlet fermions, namely right-handed Majorana neutrinos (RHNs), are added to the Standard Model in order to explain the two observed mass splittings in the active neutrino sector. These fermions are usually referred to as *sterile* neutrinos. Right-handed neutrinos are singlets of the SM gauge group, such that there is no unbroken symmetry to protect them from acquiring a large Majorana mass. Therefore, new sterile neutrinos N_i, $i = 1, 2, 3$, with Majorana mass terms M_i can be included into the SM Lagrangian. Let's assume that *sterile* neutrinos are hierarchical, such that $M_1 < M_2 < M_3$. Under this assumption, by introducing the Majorana mass term and the interaction between these sterile neutrinos and the SM lepton doublet $L_\alpha = (\nu_\alpha, l_\alpha)_L$, with $\alpha = e,\ \mu,\ \tau$, the relevant Lagrangian for the neutrino sector is given by

$$\mathcal{L}_{\text{new}} = \mathcal{L}_{\text{SM}} + i\overline{N_i}\partial\!\!\!/ N_i - \frac{1}{2}\left(\sigma y_\sigma^i \overline{N_i^c} N_i + y_\nu^{i\alpha}\overline{L_\alpha}\tilde{H} N_i + \text{h.c.}\right), \tag{2.1}$$

where y_ν is a 3×3 complex matrix representing the Yukawa couplings between sterile neutrinos and $SU(2)_L$ lepton doublet, while $\tilde{H} = i\sigma_2 H$, where $H = (H^+, H^0)$ represents the Higgs doublet. Without loss of generality, the 3×3 matrix y_σ can be chosen to be real and diagonal, so that the Majorana mass term is diagonal; the physical eigenstates of the RHNs are the Majorana neutrinos N_i, with masses $M_i = y_\sigma^i v_\sigma$, where v_σ represent the vacuum expectation value of σ. Since N_i are gauge singlets, the scale of M_i is naturally much larger than the electroweak scale $v = 246$ GeV. The electroweak (EW) symmetry is broken spontaneously when the SM Higgs doublet develops a Vacuum Expectation Value (VEV) in its the neutral component, $\langle H^0\rangle = v/\sqrt{2}$. Under this condition, one can rewrite the Lagrangian mass term for active and sterile neutrinos as

$$\mathcal{L}_{\text{mass}} = -\frac{1}{2}\begin{pmatrix}\overline{\nu_\alpha} & \overline{N_i^c}\end{pmatrix}\begin{pmatrix}0 & y_\nu^{i\alpha}\frac{v}{\sqrt{2}} \\ y_\nu^{i\alpha\dagger}\frac{v}{\sqrt{2}} & y_\sigma^i v_\sigma\end{pmatrix}\begin{pmatrix}\nu_\alpha^c \\ N_i\end{pmatrix} + \text{h.c.}\,, \tag{2.2}$$

where the Dirac mass matrix is identified as $m_D = y_\nu^{i\alpha} v/\sqrt{2}$, while the Majorana mass term is represented by $M = y_\sigma^i v_\sigma$. The diagonalization of this mass matrix will lead to the mass eigenstates of the physical particles, $U\mathcal{M}U^\dagger = \text{diag}(m_\nu, M_N)$. Hence, in the limit $m_D \ll M$, the mass matrix eigenvalues are

$$\begin{cases} m_\nu \simeq -m_D \frac{1}{M} m_D^T + \mathcal{O}(m_D^4), \\ M_N \simeq M + \mathcal{O}(m_D^4). \end{cases} \tag{2.3}$$

As has been just shown, as the Majorana mass M increases, the sterile neutrino mass M_i increases while the active neutrino mass m_{ν_α} decreases, hence the name Seesaw.

As a result, the Lagrangian of the theory can be rewritten in terms of the mass eigenstates ν_m and N_m. On the other hand, they can be related to flavor eigenstates ν_α and N_i via the mixing matrix. The relation between mass and flavor eigenstates can be derived by diagonalizing the mass matrix. Here, we analyze a simplified scenario with only one flavor to derive the general

scaling of the mixing angles. A general 2×2 mixing matrix can be defined as

$$\begin{pmatrix} \nu \\ N^c \end{pmatrix} = \begin{pmatrix} \cos\theta & -\sin\theta \\ \sin\theta & \cos\theta \end{pmatrix} \begin{pmatrix} \nu_m \\ N^c_m \end{pmatrix} , \tag{2.4}$$

where θ represent the mixing angle between the flavor and mass eigenstates. This mixing is truly represented by the mass matrix $\mathcal{M}$. For a generic 2×2 matrix, the mixing angle can be defined as

$$\begin{pmatrix} a & b \\ b & c \end{pmatrix} \Longrightarrow \tan 2\theta = \frac{2b}{a-c} . \tag{2.5}$$

Hence, for the seesaw model is described by $\tan 2\theta = -2m_D/M_M$. In the limit $m_D \ll M_M$, and imposing the relations given in Eq. 2.3, one finally obtains

$$\theta \simeq \sqrt{\frac{m_\nu}{M_N}} . \tag{2.6}$$

As $\theta \ll 1$, the mixing matrix can be expanded by using $\cos\theta \simeq 1$, $\sin\theta \simeq \theta$, and then the relation between flavor and mass eigenstates can be rewritten as

$$\begin{cases} \nu = \nu_m - \theta N^c_m , \\ N^c = \theta \nu_m + N^c_m . \end{cases} \tag{2.7}$$

This mixing allows to expand the Lagrangian in terms of the mass eigenstates. For processes whose characteristic energy E is far below the heavy scale M_i, the heavy fields N_i do not propagate on-shell. One therefore integrates them out, leading to a new non-renormalisable dimension-five operator, known as Weinberg operator,

$$\mathcal{L}_W = \frac{1}{2}(y_\nu^T M^{-1} y_\nu)_{\alpha\beta}(L_\alpha H)(L_\beta H) \; + \; \text{h.c} . \tag{2.8}$$

This dimension-five operator $LLHH$, with coefficient $\sim y_\nu^2/M$, leads to a total lepton number violation $\Delta L = 2$, which is needed in order to reproduce the neutrino masses.

This Type I seesaw mechanism is the most widely used to account for neutrino masses. Indeed, in our model we have introduced this mechanism to reproduce neutrino masses and explain a possible origin of DM. two other seesaw mechanisms can also be considered: Type II, in which neutrino masses can be generated by the tree level exchange of $SU(2)$ - triplet scalars; and Type III, which involves the introduction of $SU(2)$ - triplet fermions. Both mechanisms are beyond the scope of this work.

2.2 Inverse Seesaw mechanism

In this extension of the seesaw mechanism (see Refs. [40, 41, 42] for further details), the lepton sector of the SM is extended with two electroweak singlet leptons per generation, i.e., $L_i = (\nu_{L,i}, e_{L,i})$, $e_{R,i}$, $N_{R,i}$ and $s_{L,i}$, where $N_{R,i}$ represent the right-handed neutrinos introduced in the seesaw mechanism, while $s_{L,i}$ indicates an extra singlet, both with lepton number $L = 1$. This mechanism has also arisen in the context of left-right symmetry and SO(10) unified models.

In a basis of $(\nu^c_L, N_R, s_L)^T$ with three flavors, the 9×9 mass matrix is given by

$$\mathcal{M} = \begin{pmatrix} 0 & m_D & 0 \\ m_D^T & 0 & M^T \\ 0 & M & \mu \end{pmatrix} , \tag{2.9}$$

where m_D and M are arbitrary 3×3 complex matrices in flavor space and μ is a small lepton number violating Majorana mass term for s_L. The matrix $\mathcal{M}$ can be diagonalized by a unitary transformation, leading to nine mass eigenstates: three of them correspond to the observed light neutrinos, while the other three pairs of two component leptons combine to form three quasi-Dirac leptons. Assuming m_D, $\mu \ll M$, the effective Majorana mass matrix for active neutrinos is given by

$$m_\nu = m_D^T M^{T^{-1}} \mu M^{-1} m_D \,, \tag{2.10}$$

while the three pairs of heavy neutrinos have masses of order M, and the mixture among singlet and doublet $SU(2)$ states is suppressed by m_D/M. One can notice that in the inverse seesaw, $m_\nu \propto \mu$, such that lepton flavor and CP violation can arise even in the limit where lepton number is strictly conserved and the light neutrinos are massless, due to the mixing of the $SU(2)$ doublet neutrinos with new $SU(2) \times U(1)$ singlet leptons.

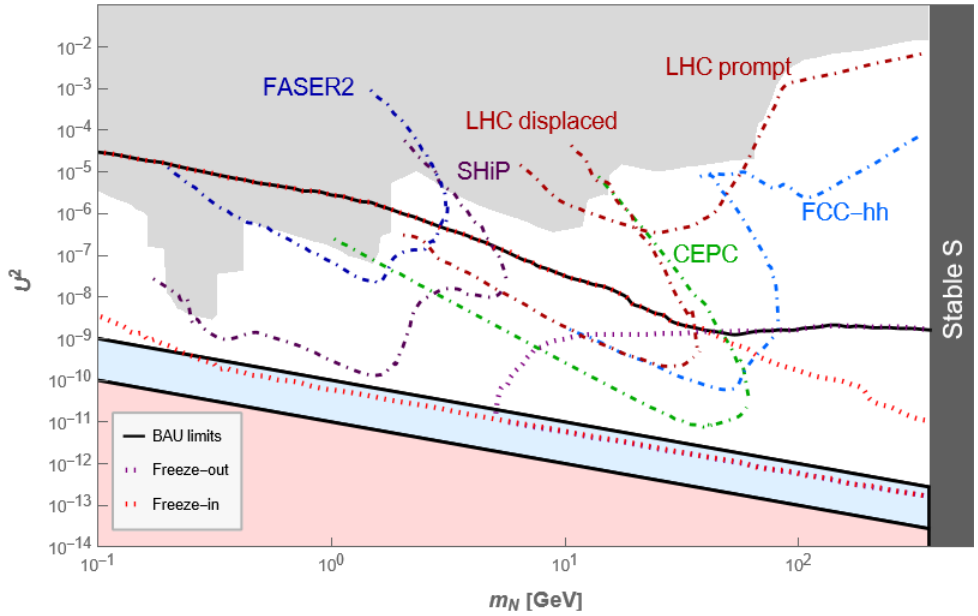

Figure 1: Range of the total mixing angle U^2 consistent with active neutrino masses as a function of RHNs mass m_N. The solid black line show the results for a vanishing initial abundance of RHNs, while the purple dotted one correspond to thermal initial conditions. The gray area indicates the experimentally excluded region. The dashed-dotted lines represent the estimated sensitivities for actual and future experiments.

The most important feature of the inverse seesaw mechanism is that as the Majorana mass term μ goes to 0, the mixing between active and sterile neutrinos can become very large, thereby opening up a much broader range of viable parameter space, as represented in Fig. 1. In this figure, obtained from previous results in Refs. [43, 44, 45, 46], we show the $U^2 - m_N$ plane, where U^2 denotes the total active–sterile mixing angle and m_N the sterile-neutrino mass. The blue band corresponds to all (U^2, m_N) points that reproduce the observed light-neutrino masses through the Type-I seesaw mechanism, that is, we reproduce the function $U^2 = m_\nu/m_N$ for 0.01 eV $\lesssim m_\nu \lesssim$ 0.1 eV, which represent the lower and upper cosmological bounds. The entire region above this band, characterized by larger mixings, becomes accessible only in the inverse-seesaw scenario.

Introducing the inverse seesaw therefore enables a detailed exploration of the low-mass regime for sterile neutrinos, as we shall discuss in Section 6.2. The dotted-dashed colored lines indicate the estimated sensitives for actual and future experiments designed for the research of physics beyond the Standard Model. In red lines it has been presented the sensitivity for the experiments LHC displaced and LHC prompt. The LHC displaced (see Ref. [47] for further details) refers to

the dedicated program at ATLAS, CMS and LHCb that targets the signatures of BSM long-lived partilces (LLPs) via displaced vertices (DVs) and missing transverse momentum, while the LHC prompt (for more detail see Ref. [48]) search program targets new particles that are produced and decay essentially at the interaction point, leaving signatures that appear "prompt" to the detectors. This experiment is focused on feebly interacting new physics.

The green line represent the CEPC Detector (see Ref. [49]), which can be divided in two phases: a circular electron-positron collider designed fer electroweak precision measurements, and a super proton-proton collider (SppC) for direct searches of new physics (expected to be constructed in 2042). The light blue line indicates the sensitivity of the detector FCC-hh (see Ref. [50] for further detail), a 100 TeV hadron-hadron collider. The darker blue line represent FASER2 (see Ref. [51]), a large-volume detector designed for sensitivity to a wide variety of models of BSM physics and for precise muon reconstruction, while SHiP (Search for Hidden Particles [52]), whose expected sensibility is presented in a purple line, is a new general-purpose experiment designed to search for any type of feebly interacting long-lived particles, that is, it is focused on the search for "hidden" particles as predicted by a large number of models of Hidden Sectors that are capable of explaining dark matter, neutrino oscillations, and the origin of the baryon asymmetry in the Universe.

3 DM production mechanisms

Since 1927, when Georges Lemaître [53] deduced the Universe's expansion from Einstein's equations of general relativity [54], physicists have been interested in studying the evolution of the abundance of particles in the Universe. In the early Universe, SM particles undergo scatterings and inelastic processes which keep them in thermal equilibrium. Thus, they can be described in terms of an interacting gas in a thermal bath in an expanding volume. Therefore, it is a good approximation to assume equilibrium dynamics, as seen in [27]. However, the expansion of the Universe leads to the departure of many particles from thermal equilibrium. The evolution of particles is described by a set of Boltzmann Equations[A].

DM can be identified with a new particle, coupled to the SM through different interactions, each of them having a different coupling. Let's consider a particle χ which interacts with an SM particle B from the thermal bath, with $m_\chi \gg m_B$. The evolution of the abundance of χ in an expanding Universe depends on the strength of these interactions. Two possible scenarios of DM production are considered (detailed for our model in Sections 5.3.1, 5.2 and 5.3.2): freeze-out and freeze-in.

3.1 Freeze-out

Let's consider a massive DM particle species χ. If these particles undergo sufficiently fast elastic scatterings with SM particles, they are kept in kinetic equilibrium with the SM bath. Hence, they can be described by an equilibrium distribution at the temperature T of the thermal bath. Namely, if both elastic (scatterings) and inelastic (annihilations) processes involving the DM particles are fast enough to maintain kinetic and chemical equilibrium, their number density follows the equilibrium distribution [27], given by

$$n_{\mathrm{eq},\chi}(T) = \frac{g_\chi m_\chi^2 T}{2\pi^2} K_2\left(\frac{m_\chi}{T}\right) = \begin{cases} g_\chi\, T^3/\pi^2\,, & T \gg m_\chi \\ g_\chi \left(\dfrac{m_\chi T}{2\pi}\right)^{3/2} e^{-m_\chi/T}\,, & T \ll m_\chi \end{cases} \tag{3.1}$$

where g_χ represents the degrees of freedom of the DM particle, and $K_2(m_\chi/T)$ is the Bessel function. In a scenario where the interaction between a fermion B from the SM bath and the dark matter particle χ is dominated by the annihilation $\chi\bar{\chi} \rightleftharpoons B\bar{B}$, and the coupling governing the interaction, λ, is large enough, χ and B were kept in thermal equilibrium in the early Universe.

More precisely, in order to understand whether a particle is kept in thermal equilibrium with the thermal bath through its interactions, it is useful to focus on the ratio Γ/H, where Γ represents the annihilation rate of the process, while H is the Hubble expansion rate. Therefore, the ratio indicates whether the interactions between particles are fast enough to maintain thermal equilibrium with the expanding bath, or if the expansion is sufficiently rapid for the particles to interact, such that an equilibrium state can no longer be sustained. To understand this, the mean free path can be introduced, $\tau = 1/n\sigma$, representing the average physical distance a particle covers between two successive interactions. Hence, as $\Gamma = v/\tau$, where v is the relative velocity between two particles, if the mean free path is less than the distance a particle travels in a Hubble time, $vH(T)^{-1}$, then $\Gamma(T) \gg H(T)$ and their interactions are sufficiently fast to maintain the equilibrium. If τ is larger than the distance, $\tau \gtrsim vH(T)^{-1}$, then $\Gamma(T) \lesssim H(T)$, leading to out-of-equilibrium dynamics.

In the case where $\Gamma \gg H$, the annihilation of the χ particles into B and the inverse process occur with the same rate, only while χ remains relativistic. Once χ becomes non relativistic, the rate for the inverse process $B\bar{B} \to \chi\bar{\chi}$ becomes much smaller than that of $\chi\bar{\chi} \to B\bar{B}$, leading to an exponentially decreasing number density of χ particles.

As a result, to study the evolution of the abundance of the χ particle, one must compute the Boltzmann equations[A] (BE) for the DM number density, taking into account the annihilation processes. Hence, one must study how the number of particles N_χ is affected by the expansion. As stated by the BE, the main parameter to focus on is the ratio Γ/H. The annihilation rate of this process is given by $\Gamma(\chi\bar{\chi} \to B\bar{B}) = \langle\sigma_{\chi\bar{\chi}\to B\bar{B}}v\rangle n_\chi$, while the Hubble parameter arises from the Friedmann equation, $H^2 = \rho/3M_{\rm Pl}^2$, where the reduced Planck mass is defined as $M_{\rm Pl} = 1/\sqrt{8\pi G} \simeq 1.22 \times 10^{19}$ GeV. Taking into account that the energy density in the radiation-dominated era is given by $\rho(T) = \frac{\pi^2}{30}g_*(T)T^4$, the Hubble expansion rate can be rewritten as

$$H(T) \simeq 1.66\sqrt{g_*(T)}\frac{T^2}{M_{\rm Pl}}\,, \tag{3.2}$$

where $g_*(T)$ represents the effective degrees of freedom at the temperature T. Entropy conservation implies that the temperature is affected by the inflation of the Universe through the relation $T \sim T_0/g_s^{1/3}a(t)$, where $a(t)$ is the scale factor of the Universe. This implies that, as the scale factor $a(t) = 1/(1+z(t))$, with $z(t)$ the redshift, increases in time, the temperature decreases as the Universe expands. As a result, by analyzing the ratio Γ/H, there can be distinguished three regions of interest, presented in Figure 2:

(I) The DM and the SM bath are in thermal equilibrium, while the DM particle is still relativistic. This regime is fulfilled as long as

$$\begin{cases} \Gamma \gg H \longrightarrow \text{Thermal Equilibrium.} \\ T \gg m_\chi \to \chi \text{ relativistic.} \end{cases} \tag{3.3}$$

At very high temperatures, $T \gg m_\chi, m_B$, the energy of each particle can be approximated by $E \sim T$, so both processes $\chi\bar{\chi} \rightleftharpoons B\bar{B}$ are kinematically allowed, leading to an equilibrium between the annihilation $\chi\bar{\chi} \to B\bar{B}$ and the inverse process $B\bar{B} \to \chi\bar{\chi}$. In other words, both processes proceed with equal rates: when a DM particle is annihilated, another one is produced via the inverse reaction. Hence, the number of χ particles in the bath remains approximately constant. As the Universe is expanding, the temperature of the thermal bath decreases, since it eventually reaches $T \sim m_\chi$, at which point the χ particle will no longer be relativistic. As the temperature drops well below m_χ, a new scenario must be taken into account, corresponding to Regime (II).

(II) Thermal equilibrium between DM and SM, with DM being non-relativistic. In this region the conditions are given by

$$\begin{cases} \Gamma \gg H \longrightarrow \text{Thermal Equilibrium.} \\ T \ll m_\chi \to \chi \text{ Non-relativistic.} \end{cases} \tag{3.4}$$

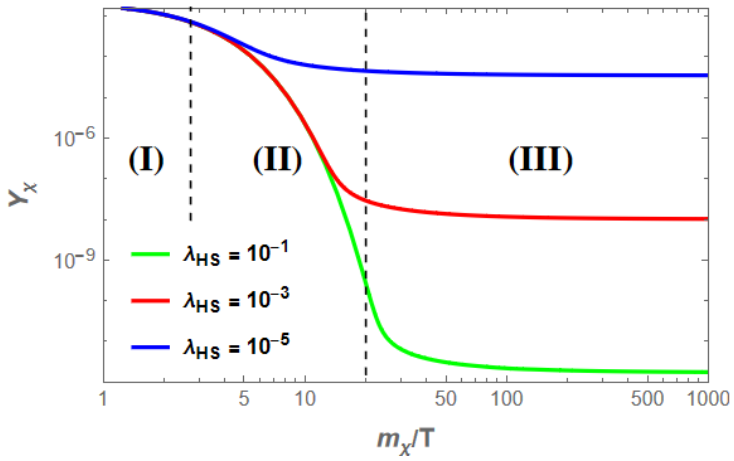

Figure 2: Evolution of the DM abundance $Y_\chi = n_\chi/s$, from solving the Boltzmann equations in the FO regime, see App. A.1. A larger coupling between χ and the SM particles leads to more effective annihilations, hence a lower relic abundance. This plot comes from solving the BE for the interaction given in Section 5.3.1.

Once the temperature is of the order of the mass of the DM particles, they become non-relativistic, so that their energy is no more proportional to the temperature of the Universe, but dominated by their mass, $E_\chi \sim m_\chi$. Nevertheless, since it is considerd $m_\chi \gg m_B$, the SM particle B is still relativistic, so its energy is given by $E_B \sim T \leq m_\chi$. Hence, as the process $B\bar{B} \to \chi\bar{\chi}$ is no more kinematically allowed, the interaction rates of both processes are no longer the same, such that the annihilation of $\chi\bar{\chi}$ begins to dominate the dynamics. However, as the energy distribution for the particles is given by the Maxwell-Boltzmann distribution, there is a small fraction of B particles, corresponding to the tail of the distribution, whose energy is $E \gg m_B$, that can still annihilate and produce a pair of DM particles. On the other hand, as $\Gamma \gg H$, the annihilation $\chi\bar{\chi} \to B\bar{B}$ occurs faster than the expansion rate. Therefore, the DM particles remains in thermal equilibrium, resulting in an exponential decrease in N_χ as $e^{-m_\chi/T}$, in accordance with Eq. 3.1. Hence, under this situation where both processes do not counter-balance each other, the abundance of DM particles begins to decrease exponentially, as can be seen in Figure 2.

Since the temperature is still decreasing, there comes a point where the annihilation rate becomes increasingly ineffective, ultimately reaching the moment when $\Gamma \sim H$, which corresponds to the so-called *freeze-out*. This situation marks the transition to Regime (III).

(III) The DM particle is non-relativistic and out of thermal equilibrium: *freeze-out*. In this region, the conditions are given by

$$\begin{cases} \Gamma < H \longrightarrow \text{Non-thermal equilibrium.} \\ T \ll m_\chi \to \chi \text{ Non-relativistic.} \end{cases} \tag{3.5}$$

In this regime, as the temperature has dropped below the DM mass m_χ, approximately when $T_{\text{fo}} \sim m_\chi/20$, the interaction rate is no longer effective compared to the expansion rate, leading to a ratio $\Gamma/H \lesssim 1$. As a result, χ and B annihilation processes are no longer significant, leading to a situation of non-interacting DM particles. Hence, as there is no particle creation neither annihilation, the DM abundance N_χ has been "frozen" at the value established by the freeze-out. This abundance is known as the relic dark matter density.

As a final point, one can analyze how the main parameters of the theory, such as the masses, temperature, and the coupling constant between the Standard Model and the new particle χ influence this relic abundance. The DM relic abundance can be determined by solving the

appropriate Boltzmann equation. However, one can provide a simple estimate based on the following argument: the DM freezes out when $\Gamma \simeq H$. Under this condition, the comoving number density $Y_\chi = n_\chi/s$ at the time of the freeze-out, $T_{\rm fo} \sim m_\chi/20$, is given by

$$Y_\chi \sim \frac{1}{M_{\rm Pl}\langle\sigma v\rangle m_\chi}\,, \tag{3.6}$$

where $M_{\rm Pl}$ represent the Planck mass. The final analytic relic abundance Ω_χ, in relation to the best-fit CDM value of the Planck satellite $\Omega_{Pl}h^2 = 0.120 \pm 0.001$, is given by (analysis done in detail at Section 5.2 for our model)

$$f_\chi \equiv \frac{\Omega_\chi h^2}{\Omega_{Pl}h^2} = \frac{m_\chi s_0 Y_\chi}{0.12\ \rho_c/h^2} = \frac{Y_\chi m_\chi}{T_{\rm eq}}\,, \tag{3.7}$$

where $s_0 \approx 2.22\cdot 10^{-38}\text{GeV}^3$ is the actual entropy density of the Universe, $\rho_c \approx 3.9\cdot 10^{-47}h^2\text{GeV}^4$ is the critical density and $T_{\rm eq} \approx 0.4\times 10^{-9}$ GeV represent the temperature at which matter and radiation contribute equally to the energy density of the Universe. With a typical weak interaction cross section $\sigma v \sim g^2/m_\chi^2$, the DM mass naturally emerges as $m_\chi \sim$ TeV.

3.2 Freeze-in

Freeze-in is an alternative DM production mechanism involving a Feebly Interacting Massive Particle (FIMP) [55]. Consider a SM particle from the bath, B, decaying into DM particles χ. In this scenario the dark-matter particle is treated as a FIMP, so extremely feeble couplings are required. Their interactions are so weak that the production rate is always smaller than the Hubble expansion rate, that is, $\Gamma \ll H$ at every stage of cosmic evolution. This condition requires a coupling $\lambda \ll \sqrt{m_\chi/M_{\rm Pl}}$. Because the interaction rate is too small to overcome the expansion of the Universe, the DM particles never reach thermal equilibrium with the SM plasma; in other words, χ remains thermally decoupled from the bath.

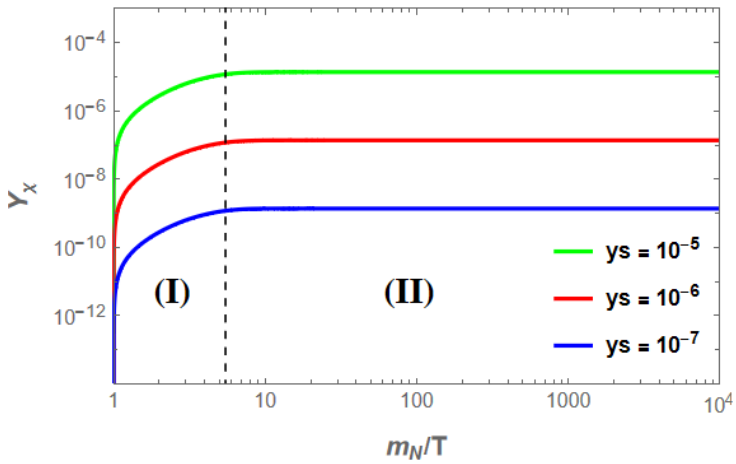

Figure 3: Evolution of the DM abundance $Y_\chi = n_\chi/s$ solving the Boltzmann equations in the FI regime, see Appendix A.2. In this case, a larger coupling between χ and SM particles leads to more effective decays of N into χ, leading to a higher relic abundance. This plot comes from solving the BE for the interaction given in Section 5.2.

On the other hand, it can be assumed that the initial DM density is negligible, $n_{\chi,0} \simeq 0$, so that annihilation processes involving χ particles can be neglected. Under this hypothesis, one can consider that the main freeze-in interactions are given by the decays $B \to \chi\chi$ or $B \to B'\chi$, where B and B' represent particles from the SM thermal bath. At early times there is no χ abundance, but the decay of B into DM begins to dominate the production, such that the

number density n_χ increases, as represented in Region (I) of Figure 3. This defines a regime in which the number of DM particles N_χ increases as the Universe expands. Once the temperature drops below m_B, and given that $m_\chi \gg m_B$, neither B nor χ remain relativistic, so that their energies become approximately proportional to their masses. Around $T \sim m_B/10$, the decay is no longer kinematically allowed, as $E_B \lesssim E_\chi$. As a result, the decay rate becomes inefficient, so that the abundance of χ "freezes-in" at a value determined by the strength of the interaction, as represented in region (II) of Figure 3. The relic abundance can be computed analytically by solving the Boltzmann equation for the decay process.

The comoving number density at present times arises from its value at $T_{\rm fi} \sim m_B/10$, which leads to

$$Y_\chi \sim \frac{M_{\rm Pl}\,\Gamma}{m_B^2}\,, \tag{3.8}$$

where Γ represents the decay rate of the given process. It can finally be related to the relic abundance Ω_χ through Eq. 3.7. The condition $\Gamma \ll H_{T\sim m_B}$ leads to an upper bound for the coupling to ensure that thermalization does not occur, constraint known as freeze-in condition (Eq. 5.7 for our model). In Section 5.2 it has been computed the freeze-in mechanism for our model, where the main interactions are given by the Lagrangian term (to see in Section 5.1) $\mathcal{L} \supset y_S S\overline{N^c}\chi$. Hence, to study this scenario for our model the decay $N \to \chi S$ is the one to be taken into account.

4 Leptogenesis

One of the outstanding questions in modern cosmology and particle physics is the origin of the baryon asymmetry of the Universe[1,2], namely, the observed excess of matter over antimatter. While the Standard Model provides the ingredients for baryon number violation and CP violation established by Sakharov conditions, it fails to generate a sufficient asymmetry through electroweak baryogenesis alone. This has motivated the exploration of mechanisms beyond the Standard Model that are that are capable of generating the observed baryon asymmetry. One of the most popular theories to generate the matter-antimatter asymmetry is leptogenesis (see Refs. [4, 6, 8, 13, 14] for further details).

Leptogenesis is a particularly appealing scenario that addresses this problem, providing a mechanism where a lepton asymmetry is generated in the early Universe, which is subsequently converted into a baryon one via non-perturbative electroweak processes known as sphalerons [34]. This mechanism not only explains the BAU, but is also naturally connected to the generation of neutrino masses through the seesaw mechanism, offering a unified framework for two fundamental open problems in physics.

In its minimal version, leptogenesis arises in type-I seesaw models, where the the decay of RHNs out-of-thermal equilibrium leads to lepton number and CP violation. Depending on the mass scale of the right-handed neutrinos, various leptogenesis scenarios can be realized, such as thermal leptogenesis, resonant leptogenesis, or low-scale flavored leptogenesis with oscillations.

4.1 Thermal leptogenesis

The most common framework is *thermal leptogenesis*,in which heavy Majorana neutrinos are produced via scatterings in the thermal bath starting from a vanishing initial abundance, so that their number density can be calculated solely in terms of the seesaw parameters and the reheating temperature of the Universe. Indeed, two different scenarios can be considered: one in which the initial abundance of N_i is vanishing, and another where the sterile neutrinos have been part of the thermal bath since the early Universe. Let's consider three families of sterile neutrinos N_i, with masses M_1, M_2 and M_3. In order to reproduce the lepton asymmetry and the light neutrino mass scale with perturbative Yukawa couplings y_ν via thermal leptogenesis, a large amount of

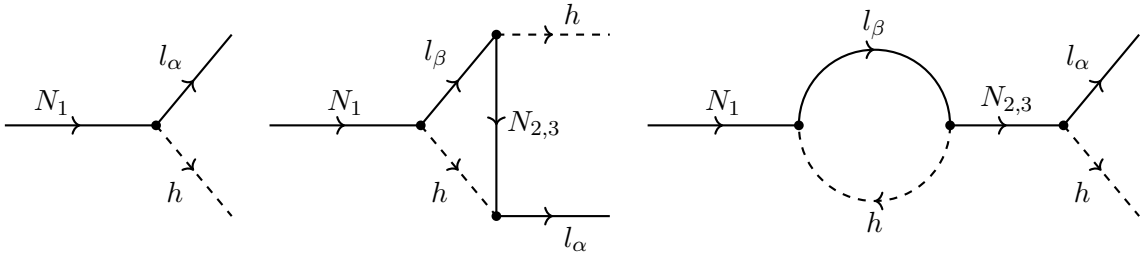

Figure 4: Decay $N_1 \to lh$ at tree-level and loop corrections, where the third diagram correspond to the self-energy correction. The interference of this diagrams leads to the CP asymmetry

CP asymmetry is required, which leads to the Davidson-Ibarra bound 10^9 GeV $\lesssim m_N$ [56]. On the other hand, an upper bound $m_N \lesssim 10^{15}$ GeV arises from requirement of perturbative Yukawa couplings. Hence, in order to study thermal leptogenesis, three main assumptions are made:

1) The RHN masses are hierarchical: $10^9 \lesssim M_1$ GeV $\ll M_2$, M_3.

2) Thermal production of N_1 and negligible initial abundance of N_2 and N_3.

3) Lepton asymmetry is produced in a single flavor.

Given that only the right-handed neutrino N_1 has an initial thermal abundance, our analysis can be restricted to interactions involving this one RHN. When the temperature of the Universe drops below M_1, the sterile neutrino N_1 begins to decay into leptons (see Figure 4), such that the equilibrium number density of the N_1 population is exponentially suppressed $\propto e^{-M_1/T}$. If the decay of N_1 occurs in equilibrium, the abundance, and hence the resulting asymmetry, will be strongly suppressed, since the decay is produced at $T < m_N$. However, if the decay occurs out of equilibrium, the resulting abundance and CP asymmetry are no longer exponentially suppressed, allowing for the generation of a baryon asymmetry consistent with observations. Hence, when N_1 decays are produced out-of-equilibrium, the lepton asymmetry from the decays may survive, leading to a baryon asymmetry that can be approximated as [6]

$$Y_{\Delta B} \simeq \frac{135\zeta(3)}{4\pi^4 g_*}\epsilon_1 \times \eta \times \mathcal{C}\,, \tag{4.1}$$

where ϵ_1 represent the CP asymmetry produced in N_1 decay, η is the efficiency factor that quantifies the departure from equilibrium, and $\mathcal{C}$ accounts for the conversion of lepton asymmetry into baryon asymmetry via sphaleron processes. Hence, in order to reproduce the BAU, these three parameters must be computed.

4.1.1 CP-violation

In order to produce a net lepton asymmetry, there must be lepton number-violating interactions of the sterile neutrino N_1, allowing one to define the CP asymmetry as the difference between the production rates of leptons and antileptons,

$$\epsilon_{1\alpha} \equiv \frac{\Gamma(N_1 \to l_\alpha h) - \Gamma(N_1 \to \bar{l}_\alpha \bar{h})}{\Gamma(N_1 \to l_\alpha h) + \Gamma(N_1 \to \bar{l}_\alpha \bar{h})}\,. \tag{4.2}$$

Hence, it can be shown that the CP asymmetry does not come from different decay rates in the production of leptons and antileptons at tree level, but instead arises from the interference of tree-level and one-loop amplitudes (for more detail, see Refs. [6, 15, 8]). At tree level, the decay width of N_1 is given by $\Gamma(N_1 \to l_\alpha h) = {\lambda_1^\alpha}^2 M_1/8\pi$, where λ_1^α represents the coupling between N_1 and the SM lepton l_α. Letting $\lambda_{2,3}^\alpha$ denote the coupling of the lepton l_α to N_2 and N_3, the total decay width can be expressed as

$$\Gamma(N_1 \to l_\alpha h) \propto |\lambda_1^\alpha + A\lambda_1^\beta \lambda_{2,3}^\beta \lambda_{2,3}^\alpha|^2\,, \qquad \Gamma(N_1 \to \bar{l}_\alpha \bar{h}) \propto |\lambda_1^{\alpha *} + A^* \lambda_1^\beta \lambda_{2,3}^{\beta *} \lambda_{2,3}^{\alpha *}|^2\,, \tag{4.3}$$

where A denotes the complex CP-conserving loop factor. In the limit $M_{2,3} \gg M_1$ (assumption 1), the one-loop diagrams introduce a suppression in A proportional to $1/M_{2,3}$, arising from the heavy mediators $N_{2,3}$. Since the intermediates states in the loop can go on shell, the Optical Theorem guarantees that A has an imaginary part, which, when combined with complex couplings, enables the CP violation relevant for our scenario. From now on, it has been considered only one SM lepton flavor (assumption 3), allowing us to omit the index α. Therefore, the CP-asymmetry can be rewritten as

$$\epsilon_1 \simeq \frac{3}{16\pi}\frac{M_1}{M_{2,3}}\mathrm{Im}\{\lambda_{2,3}^2\}\,. \tag{4.4}$$

The Davidson-Ibarra bound comes from imposing a lower limit on $|\epsilon_1|$. The requirement that the predicted baryon asymmetry matches the observed value in Eq. 1.7 implies $\epsilon_1 \gtrsim 10^{-6}$, which in turn leads to $M_1 \gtrsim 10^9$ GeV.

4.1.2 Efficiency factor

The non-equilibrium situation necessary for thermal leptogenesis is provided by the expansion of the Universe, as those interaction rates that are of the same order as, or slower than, Hubble expansion rate are not fast enough to equilibrate particle distributions. Given that the timescale of leptogenesis is H^{-1}, there can be neglected interactions that are much slower than H, while interactions whose rates are faster than the expansion impose chemical and kinetic equilibrium conditions on particle distributions. Thus, the efficiency factor estimates the amount of interactions produced in an out-of-equilibrium scenario, whose contributions are crucial for the leptogenesis.

On the one hand, in the limit of N_1 interactions in perfect equilibrium, one finds out that $\eta = 0$, meaning that no asymmetry is created. On the other hand, when the decays occur in an out-of-equilibrium situation, one can define the ratio (see Ref. [15])

$$R \equiv \left.\frac{\Gamma_1}{H(T)}\right|_{T\sim M_1} \sim \frac{\tilde{m}_1}{\tilde{m}^*}\,, \tag{4.5}$$

where $\tilde{m}^* \equiv \frac{256\sqrt{g_{SM}}v^2}{3M_{\rm Pl}} \simeq 2.3\cdot 10^{-3}$ eV, with $g_{SM} = 118$ denoting the number of degrees of freedom of SM particles, while $\tilde{m}_1 \equiv \lambda_1^2 v^2/M_1$ represents the contribution to the light neutrino mass mediated by N_1. Thus, if $R \ll 1$, N_1 decays are strongly out-of-equilibrium and then $\eta = 1$, whereas if $R \gg 1$, the decay of N_1 occurs mostly in equilibrium, so that the lepton asymmetry is suppressed as $\eta \sim 1/R$.

Furthermore, certain processes can wash out the lepton asymmetry that has been generated. In particular, reactions mediated by the virtual exchange of $N_{1,2,3}$ violate lepton number by two units ($\Delta L = 2$) and therefore reduce the total lepton asymmetry. These scatterings cause a strong exponential suppression of the baryon symmetry, as their rates are not Boltzmann suppressed at $T \lesssim M_1$.

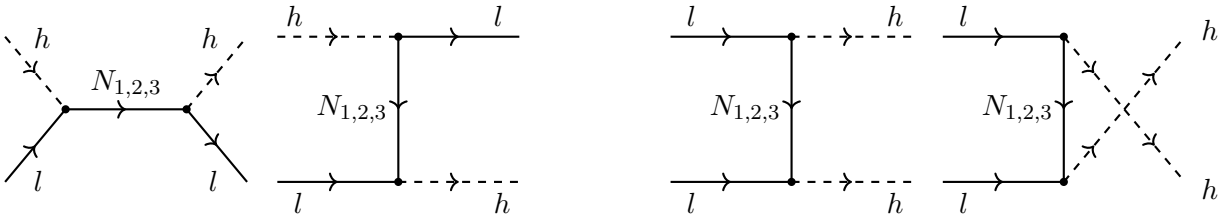

Figure 5: Washout process $lh \leftrightarrow \overline{l}\overline{h}$ (left pannel) and $ll \leftrightarrow h\bar{h}$ (right pannel). Both scatterings contribute with $\Delta L = 2$.

Eventually, the efficiency factor can be computed depending on the initial abundance of N_1:
• If N_1 has a thermal initial abundance, the efficiency factor is given by

$$\eta \sim \min\Big(1, \frac{\tilde{m}^*}{\tilde{m}_1}\Big)\,. \tag{4.6}$$

• If N_1 has a negligible initial abundance at $T \gg M_1$, its abundance at $T \sim M_1$ would be suppressed by $\tilde{m}_1/\tilde{m}^*$. Hence, the efficiency factor is given by

$$\eta \sim \min\Big(\frac{\tilde{m}_1}{\tilde{m}^*}, \frac{\tilde{m}^*}{\tilde{m}_1}\Big)\,. \tag{4.7}$$

• If N_1 initially dominates the energy density of the Universe, the efficiency factor is given by

$$\eta \sim \min\Big(g_{SM}, \frac{\tilde{m}^*}{\tilde{m}_1}\Big)\,. \tag{4.8}$$

4.1.3 Lepton and $B + L$ violation

Once the CP-asymmetry and the efficiency factor have been computed, it is necessary to determine how the baryon asymmetry can be obtained from the lepton one generated by the decays of N_1. Baryon number violation is provided by $\mathcal{B} + \mathcal{L}$ violating non-perturbative SM processes (See Section 3 from Ref. [6] for more details). Since $\mathcal{B} - \mathcal{L}$ is not affected by these sphaleron processes, it is sufficient to determine how thermal equilibrium processes affect the violation of $\mathcal{B}$ and $\mathcal{L}$ individually, and relate them through the conserved quantity $\mathcal{B} - \mathcal{L}$.

In the early Universe, particles were in thermal equilibrium, so that their primordial asymmetries were encoded in their chemical potentials, assuming $\mu \ll T$, as

$$n_i - \bar{n}_i \propto \mu_i T^2\,. \tag{4.9}$$

Therefore, lepton and baryon asymmetries can be expressed in terms of particle's chemical potentials. Up to this point, one can consider that each particle carries an asymmetry A_P such that $\mu_P \equiv A_P/g_P$, where g_P is the number of internal degrees of freedom. By imposing that the interactions in the early Universe equilibrate the chemical potentials of the particles through different processes, one can relate the various asymmetries.

Let us consider the main interactions arising from the Lagrangian of the theory, which impose several constraints over the chemical potential of the relevant particles. On the one hand, the SM matter content is $P = \{L,\ R,\ Q,\ U,\ D,\ H\}$, where $L \equiv$ Left-handed fermion doublet (ν_L, l_L); $\overline{R} \equiv$ Right-handed fermion singlet l_R; $Q \equiv$ Left-handed quark doublet (u_L, d_L); $\bar{U}/\bar{D} \equiv$ Right-handed up/down type quark u_R/u_R; and H represents the Higgs doublet. On the other hand, the equilibration of the chemical potential through the dominant interactions in the theory leads to a system of equations:

$$\begin{cases} \text{Yukawa: } LHR \longrightarrow & 0 = \mu_R + \mu_L + \mu_H \\ \text{Yukawa: } HQD \longrightarrow & 0 = \mu_D + \mu_Q + \mu_H \\ \text{Yukawa: } \bar{H}QU \longrightarrow & 0 = \mu_U + \mu_Q - \mu_H \\ \text{Sphaleron: } QQQL \longrightarrow & 0 = 3\mu_Q + \mu_L \\ \text{Neutrality: } \sum_i Y_i\mu_i d_i = 0 \longrightarrow & 0 = N_{gen}(\mu_Q - 2\mu_u + \mu_D - \mu_L + \mu_R) - 2N_{Higgs}\mu_H. \end{cases}$$

Here, Y_i denotes the hypercharge of each particle specie, with d_i the degrees of freedom, which are related to the number of generations N_{gen}. Up to this point, using the definition of the asymmetry in a particle P as $A_P = \mu_P\, g_P$, the baryon and lepton asymmetry can be written as

$$B = \mu_Q g_Q - \mu_U g_U - \mu_D g_D = 3(2\mu_Q - \mu_U - \mu_D), \tag{4.10}$$

$$L = \mu_L g_L - \mu_R g_R = 3(2\mu_L - \mu_R), \tag{4.11}$$

$$(B - L) = 3(2\mu_Q - \mu_U - \mu_D - 2\mu_L + \mu_R). \tag{4.12}$$

Under these conditions, chemical potentials can be solved in terms of a single parameter. Therefore, one can finally arrive to an expression relating the lepton and baryon asymmetries as

$$B = \frac{28}{79}(B-L), \qquad L = -\frac{51}{29}(B-L)\,. \tag{4.13}$$

As a result, the coefficient relating the B and $B-L$ asymmetry is given by $\mathcal{C} = \frac{28}{79}$.

Under this assumptions, the observed baryon asymmetry can be successfully reproduced for $M_1 \gtrsim 10^9$ GeV. However, new considerations must be taken into account in order to reproduce the observed asymmetry for lighter RHNs.

4.2 Resonant leptogenesis

As discussed in the previous Section, leptogenesis was originally proposed by Fukugita and Yanagida for heavy right-handed neutrinos with masses above 10^9 GeV (Davidson-Ibarra bound). This mass scale can be significantly lowered if two sterile neutrinos are nearly degenerate in mass, a framework known as *resonant leptogenesis* (see Refs. [43, 44, 45, 46, 57] for further details).

In this scenario, a resonant enhancement of the CP asymmetry in N_1 decays occurs when the mass difference between N_1 and N_2 is of the order of their corresponding decay widths, that is,

$$|M_1 - M_2| = \frac{\Gamma_{N_2}}{2}\,. \tag{4.14}$$

Here Γ_{N_2} denotes the decay rate of the process involving N_2. In such a case, the resonant effect is related to the self energy contribution to the CP asymmetry, represented by the third diagram in Figure 4. The self-energy contribution involving the intermediate N_2 to the total CP asymmetry is given by (see Eq. 1.120 from Ref. [8])

$$\epsilon_1(\text{self-energy}) = -\frac{M_1}{M_2}\frac{\Gamma_{N_2}}{M_2}\frac{M_2^2(M_2^2-M_1^2)}{(M_2^2-M_1^2)^2+M_1^2\Gamma_{N_2}^2}\frac{\text{Im}[(\lambda_1^\dagger\lambda_2)^2]}{(\lambda_1^\dagger\lambda_1)(\lambda_2^\dagger\lambda_2)}\,, \tag{4.15}$$

where by applying the resonance condition in Eq. 4.14, the CP asymmetry can be rewritten as

$$|\epsilon_1(\text{resonance})| \simeq \frac{1}{2}\frac{\text{Im}[(\lambda_1^\dagger\lambda_2)^2]}{(\lambda_1^\dagger\lambda_1)(\lambda_2^\dagger\lambda_2)}\,. \tag{4.16}$$

In the resonant case, the asymmetry is not suppressed by the smallness of the light neutrino masses, nor the smallness of their mass splitting and neither the small ratios between the singlet neutrino masses. This contrasts with the standard case, where the CP asymmetry is suppressed by large masses $M_{2,3}$, as shown in Eq. 4.4. The fact that a large asymmetry can be generated independently of the singlet neutrino masses opens the possibility for low-scale resonant leptogenesis.

In this framework, the BAU is generated when the temperature drops below the mass of the lightest neutrino, $T \lesssim M_{N_1}$, and the RHNs begin to decay out of equilibrium. On the other hand, since the conversion between lepton and baryon number requires fast electro-weak sphaleron processes, this implies a lower bound on the lightest neutrino mass around $M_{N_1} \sim T_{sph} \simeq 130$ GeV. Therefore, resonant leptogenesis allows for the study of baryogenesis in the mass range 10^2 GeV $\lesssim m_N \lesssim 10^6$ GeV, as illustrated in Figure 8. The parameter space can be further enlarged to smaller neutrino masses, 10^{-1} GeV $\lesssim m_N \lesssim 10^2$ GeV, considering leptogenesis with oscillations (beyond the scope of this work).

5 Our model

The necessary framework to understand our model has been established. In Section 1, it was discussed the main shortcomings of the SM and the motivation for developing BSM theories. Section 2 presented the theoretical framework incorporating right-handed neutrinos, which are essential to our model. Furthermore, Section 3 focused on the main DM production mechanisms, whereas Section 4 outlined the theoretical background required to account for the observed baryon asymmetry. Once the framework has been introduced, one may focus on the Dark Sector and its interactions.

This work is based on the model proposed by Juan Herrero García, Giacomo Landini & Tsutomu T. Yanagida [1], with the aim of performing a low-energy analysis to study the behavior of the model in the regime of lighter right-handed neutrino masses. First of all, in Section 5.1 it will be included the Dark Sector for this model and its main interactions with the SM. As will be shown, the interaction Lagrangian of the model leads to different DM production scenarios depending on the values of the couplings.

On the one hand, we will consider values of y_S small enough that χ never thermalizes through its interactions with N. Therefore, the production of χ particles will be studied in the freeze-in framework, as presented in Section 5.2. On the other hand, the production of S particles can be divided into two scenarios depending on the strength of the coupling λ_{HS}. First, in Section 5.3.1 we will assume $\lambda_{HS} \sim \mathcal{O}(1)$, such that S efficiently thermalizes with the SM bath through its interaction with the Higgs and undergo the freeze-out dynamics discussed in Section 3.1. Furthermore, in Section 5.3.2, it will be considered the case in which the Higgs-portal coupling λ_{HS} is feebly enough that thermalization between S and H does not occur, leading to a freeze-in scenario for S production. Finally, in Section 5.4, we will study the late decay $S \to \chi\nu$ and its consequences, with the corresponding cosmological constraints presented in Section 5.5.

5.1 Dark Sector

As presented in Section 1.3, the existence of dark matter is one of the most compelling indications of the need for new physics BSM. Right-handed neutrinos are a highly motivated extension to the SM, often considered to be responsible for the generation of neutrino masses and the matter-antimatter asymmetry of the Universe. It is thus natural to ask whether they could also be related to dark matter and whether they can account for the observed DM abundance in the Universe.

The simplest possibility is that, given an appropriate mass and sufficiently small mixing, sterile neutrinos themselves could constitute DM, produced via the Dodelson–Widrow or Shi–Fuller mechanism (see Refs. [58, 59] for further details). However, bounds on the radiative decays of RHNs into gamma rays place severe constraints on the parameter space where they can be interpreted as DM. Indeed, sterile neutrinos could only be viable DM if their mass lies around the keV range; for higher masses, the predicted lifetimes become too short to be compatible with observations.

Therefore, it is reasonable to go beyond this minimal scenario and introduce a new dark sector into the SM. Given the singlet nature of sterile neutrinos under the SM gauge symmetries, they can readily couple to the dark sector, giving rise to new interactions that may explain the origin, production, and present-day abundance of DM, as well as its role in the evolution of the Universe (see Refs. [60, 61, 62, 63] for more detail).

As a result, one may be interested in the simplest extension of this scenario that incorporates DM [1], ideally in a way that directly links it to the generation of active neutrino masses m_ν and the BAU. The minimal setup for a portal between RHNs and DM involves the introduction of a Majorana singlet fermion χ, with a Majorana mass m_χ. Moreover, with only interactions involving SM fields, it becomes challenging to generate the correct relic abundance for the fermion χ. Therefore, an additional complex scalar dark singlet S, with mass m_S, must be introduced.

In principle, both χ and S could be DM candidates; however, for definiteness, it is considered $m_\chi < m_S$, such that the fermion plays the role of DM candidate. The dark sector has been summarized in Table 1.

Particle	**Notation**	$U(1)_{B-L}$	P_M
Right-handed neutrinos	N_i	-1	$-$
SM Higgs doublet	H	0	$+$
Scalar singlet	σ	2	$+$
Dark Majorana fermion	χ	0	$+$
Dark scalar singlet	S	$+1$	$-$

Table 1: Particle content of this model. The third column indicates the charges under $U(1)_{\mathrm{B-L}}$, while the remnant matter parity $P_M = (-1)^{\mathrm{B-L}}$ is represented in fourth column. Standard Model leptons have $B - L = -1$, while quarks have $B - L = 1/3$.

On the one hand, the main interactions of these dark fermions are given by its coupling to the dark scalar and to the sterile neutrino, parametrized by

$$-\mathcal{L}_\chi \supset \frac{1}{2} m_\chi \overline{\chi^c}\chi + y_S S \overline{N^c}\chi + \text{h.c.}\,, \tag{5.1}$$

where y_S is a complex vector of Yukawa couplings between the Dark Sector and the RHNs. On the other hand, the dark scalar interacts with the Higgs doublet via Higgs-portal interactions, mediated by the coupling constant λ_{HS}. Hence, the relevant terms in the scalar potential are

$$-\mathcal{L}_S \supset m_S^2 S S^\dagger + \lambda_{HS}|H|^2 S S^\dagger + \ldots \tag{5.2}$$

Under this new interactions, and taking into account the interactions terms from the seesaw model in Eq. 2.1, where L represents the SM lepton doublet, the full Lagrangian of the theory is given by

$$\mathcal{L} = \mathcal{L}_{\mathrm{SM}} + \mathcal{L}_{\mathrm{mass}} - y_\nu \overline{L}\tilde{H} N - y_S S \overline{N^c}\chi - \lambda_{HS}|H|^2 S S^\dagger + h.c.\,, \tag{5.3}$$

with $\mathcal{L}_{\mathrm{mass}} = -m_s^2 S S^\dagger - \frac{1}{2} m_\chi \overline{\chi^c}\chi - \frac{1}{2} M_N \overline{N^c} N$. After the electroweak symmetry breaking, the Higgs obtains a VEV, such that the Higgs doublet can be expanded as $H = \frac{1}{\sqrt{2}}(v+h)\begin{pmatrix} 0 \\ 1 \end{pmatrix}$, where $v = 246$ GeV. Thus, rewriting the relevant terms into the Lagrangian, one can finally obtain

$$\mathcal{L} = \mathcal{L}_{\mathrm{SM}} + \mathcal{L}_{\mathrm{mass}} - \frac{1}{\sqrt{2}} y_\nu \overline{\nu_L}(v+h) N - y_S S \overline{N^c}\chi - \frac{1}{2}\lambda_{HS} h^2 S S^\dagger\,. \tag{5.4}$$

With the mixing between flavor and mass eigenstates in Eq. 2.7, the Lagrangian be expanded in powers of the mixing angle θ. At the leading order for $\theta \ll 1$ one obtains

$$-\mathcal{L}_{\mathrm{int}} = \frac{1}{\sqrt{2}} y_\nu \overline{\nu_L}(v+h) N + y_S S \overline{N_m^c}\chi + y_S \theta S \overline{\nu_m^c}\chi + \frac{1}{2}\lambda_{HS} h^2 S S^\dagger\,. \tag{5.5}$$

This Lagrangian gives rise to three type of interactions between the SM and the dark sector, each corresponding to a different scenario in the Universe depending on the values of the couplings and particle masses. Therefore, in the following section it will be studied the different mechanisms of DM production from right-handed neutrinos, always in the limit $m_N \gg m_\chi, m_s$ (heavy ν_R limit).

5.2 Production of χ: Freeze-in decay $N \to \chi S$

As established in Section 3.2, the freeze-in mechanism occurs when the interactions between DM and the SM are too weak to bring dark matter into thermal equilibrium with the SM bath. This implies very small couplings between DM and the SM bath particles. Under this hypothesis, the main interaction that must be taken into account in our model is given by $\mathcal{L}_{int,FI} = y_s S \bar{N}^c \chi$, where y_s is the Yukawa coupling between the dark sector particles S, χ and the sterile neutrino N. This interaction leads to the decay of the sterile neutrino to DM, with the corresponding Feynman diagram shown in Figure 6. The aim of this Section is to compute the relic dark

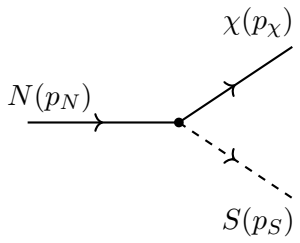

Figure 6: Decay $N \to \chi + S$

matter abundance $\Omega_\chi h^2$, produced by the decays of N, with decay rate $\Gamma(N \to \chi S)$. The decay is kinematically allowed only under the condition $m_N \gg m_\chi, m_S$. In such a case, the differential decay rate in the right-handed neutrino rest frame is given by

$$d\Gamma(N(p_N) \to \chi(p_\chi) S(p_S)) = \frac{1}{2m_N}(2\pi)^4 \delta^4(p_N - p_\chi - p_S) \frac{d^3 p_\chi}{(2\pi)^3 2E_\chi} \frac{d^3 p_S}{(2\pi)^3 2E_S} \overline{|\mathcal{M}|^2}\,, \tag{5.6}$$

where $\overline{|\mathcal{M}|^2}$ represent the spin-averaged squared amplitude of the process, and p_N, p_χ and p_S are the respective momenta of N, χ, and S. The computation of the decay rate has been done in Appendix B.1. Therefore, on can obtain theoretically the decay rate of the process, given by Eq. B.4. By imposing $\Gamma < H$, one obtains, for the freeze-in temperature $T_{\rm fi} \simeq m_N/3$, that the FI condition establishes an upper bound for the Yukawa coupling,

$$y_S^2 \lesssim \frac{16\pi^2}{27} \sqrt{\frac{g_*(T_{\rm fi})}{10}} \frac{m_N}{M_{\rm Pl}}\,. \tag{5.7}$$

However, the physical quantities of interest are comoving number density $Y_\chi \equiv \frac{n_\chi}{s}$ and the ratio of the DM abundance $f_\chi \equiv \frac{\Omega_\chi h^2}{\Omega_{Pl} h^2}$, which are given by Eqs. B.6 and B.7. On the one hand, the comoving number density for the process is given by

$$Y_\chi \simeq 1.44 \times 10^{-5} \left(\frac{y_S}{10^{-5}}\right)^2 \left(\frac{10^9 \text{ GeV}}{m_N}\right), \tag{5.8}$$

$$f_\chi \simeq \left(\frac{m_\chi}{2.77 \times 10^{-5} \text{ GeV}}\right) \left(\frac{y_S}{10^{-5}}\right)^2 \left(\frac{10^9 \text{ GeV}}{m_N}\right). \tag{5.9}$$

With these results, by properly fixing the values of the masses m_N and m_χ, and the value of the coupling constant y_S, one can reproduce the desired value of the dark matter abundance ratio f_χ, a result to be seen in Section 6.

5.3 Production of S

The main interactions for the dark scalar S are given by the Lagrangian in Eq. 5.2, where it can be seen that the scalar is coupled to the SM through the Higgs-portal. After the electroweak symmetry breaking, the Higgs adquires a VEV $v = 246$ GeV, such that the Higgs-portal

interaction can be expanded as

$$\mathcal{L}_{\mathcal{H}-\mathcal{S}} = \frac{\lambda_{HS}}{2} SS^\dagger hh + \frac{\lambda_{HS}}{2} v^2 SS^\dagger + \lambda_{HS} v SS^\dagger h \,. \tag{5.10}$$

As can be seen, three new possible interactions between S and the Higgs boson h arise, each dominating depending on the value of the coupling λ_{HS}. The Higgs boson mass is given by $m_h = (125.11 \pm 0.11)$ GeV [64]. Through the Higgs portal, we can study two distinct scenarios for the production of S particles. First, in Section 5.3.1, we examine the case where the coupling is large enough to bring S into thermal equilibrium with the SM thermal bath, leading to its production via the freeze-out mechanism. On the other hand, if the coupling is too weak to thermalize S, this opens the possibility of studying the abundance of S within a freeze-in scenario, which is analyzed in Section 5.3.2.

5.3.1 Freeze-out: Scattering $SS^\dagger \to hh$

As discussed in Section 3.1, the freeze-out framework is realized when the interaction rate of a given process is efficient enough to maintain thermal equilibrium between the particle and the SM thermal bath. In this regime is considered $\lambda_{HS} \sim \mathcal{O}(1)$.Hence, as λ_{HS} is sufficiently large, it ensures that $\Gamma \gg H(T)$ at early times, that is, the Higgs-portal induces thermalization between S and H, placing the system in the freeze-out regime.

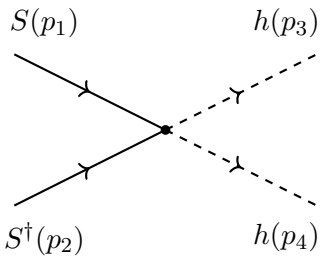

Figure 7: Higgs portal interaction, whose main contribution is given by the scattering $SS^\dagger \to hh$. The computation of this scattering establishes the evolution of the number density n_S, in the FO regime.

For $m_S \gg m_h$ the dominant process is the scattering $SS^\dagger \to hh$, whose Feynman diagram is shown in Figure 7. Since the evolution of n_S, the number density of S particles, is dominated by this scattering, one need to compute the thermal average of the scattering cross section, $\langle \sigma v \rangle$, and finally obtain the number density of particles in a comoving volume at the moment of the freeze-ou, $Y_{S,\infty} = n_S/s\,|_{T_{\rm fo}}$.

For the process $S(p_1)S^\dagger(p_2) \to h(p_3)h(p_4)$, the differential cross section is given by

$$d\sigma = (2\pi)^4 \delta^{(4)}(P_i - P_f) \frac{1}{4I} |M_{fi}|^2 \frac{d^3p_3}{(2\pi)^3 2E_3} \frac{d^3p_4}{(2\pi)^3 2E_4} \,, \tag{5.11}$$

where I represents the flux factor, defined in Eq. B.9. By solving the phase space integrals, one obtains the cross section for the process as (see Appendix B.2 for further details)

$$\sigma v_{rel} = \frac{|\lambda_{HS}|^2}{64\pi m_s^2} \sqrt{1 - \frac{m_h^2}{m_s^2}} \,, \tag{5.12}$$

where v_{rel} denotes the relative velocity between the two incoming particles. The annihilation rate can be related with the cross section by $\Gamma \sim n_\chi \langle \sigma v_{rel} \rangle = s Y_{S,\infty} \langle \sigma v_{rel} \rangle$, where the number density of the dark matter at the moment of the freeze-out is given by Eq. 3.1, at the regime

$T \ll m_\chi$. The entropy at the early Universe can be expressed in terms of the temperature and the effective number of degrees of freedom as

$$s(T) = \frac{2\pi^2}{45} g_{*s}(T) T^3 \,. \tag{5.13}$$

Finally, based on the solutions for $Y_{S,fo} \equiv \frac{n_S}{S}\Big|_{T_{\rm fo}}$ and $f_{S,fo} = \frac{Y_{S,fo} \cdot m_S}{T_{\rm eq}}$ presented in Eq. B.17 and Eq. B.18 respectively, we can rewrite them as

$$Y_{S,\rm fo} \simeq 1.74 \times 10^{-13} \left(\frac{m_S}{400\ \text{GeV}}\right)\left(\frac{0.3}{\lambda_{HS}}\right)^2 , \tag{5.14}$$

$$f_{S,\rm fo} \simeq 0.012 \left(\frac{m_S}{400\ \text{GeV}}\right)^2 \left(\frac{1}{\lambda_{HS}}\right)^2 . \tag{5.15}$$

These expressions allow us to analytically determine the present-day relative abundance of S resulting from its production via freeze-out scattering.

5.3.2 Freeze-in: Decay $h \to SS$

One may finally wonder what would happen if the Higgs-portal coupling λ_{HS} were not strong enough to allow for thermalization between S and H. In such scenario, the main interaction induced by the Higgs portal is no longer the scattering $SS^\dagger \to hh$, but instead the decay $h \to SS$ dominates the dynamics, induced by the Lagrangian term $\mathcal{L} \supset \lambda_{HS} v S S^\dagger h$. The analysis of this decay has been carried out the freeze-in regime, following the treatment in Ref. [65] in . The decay $h \to SS$, whose Feynman diagram is similar to that shown in Figure 6, is kinematically allowed if $m_h > 2m_S$. Following the same procedure as in Section 5.2, the spin-averaged squared amplitude is given by $\overline{|\mathcal{M}|^2} = \frac{1}{2}|\mathcal{M}|^2$, where $|\mathcal{M}|^2 = |\lambda_{HS}|^2 v^2$, as derived from the Feynman vertex contribution. Hence, the decay rate can be computed from Eq. B.2, substituting m_N for m_h, and using the center-of-mass momentum $p_{CM} = \frac{m_h}{2}\sqrt{1 - \frac{4m_S^2}{m_h^2}}$. This yields to

$$\Gamma_{h\to SS} = \frac{\lambda_{HS}^2 v^2}{16\pi m_h} \sqrt{1 - \frac{4m_S^2}{m_h^2}} \,. \tag{5.16}$$

By applying the FI condition $\Gamma \lesssim H(T_{\rm fi})$, where $H(T)$ is given by Eq. 3.2 and $T_{\rm fi} \sim \frac{m_h}{3}$, thermalization is avoided as long as

$$|\lambda_{HS}|^2 \lesssim \frac{1.66 \cdot 16\pi\sqrt{g_*}}{9v^2} \frac{m_h^3}{M_{\rm Pl}} \left(1 - \frac{4m_S^2}{m_h^2}\right)^{-1/2} . \tag{5.17}$$

On the other hand, from the definition of Y_S in Eq. B.6, and using the expression for $\Gamma_h \to SS$ in Eq. 5.16, the comoving number density $Y_{S,fi}$ and the ratio of the relic S abundance $f_{S,fi}$ are given, for $m_S \ll m_h$, by

$$Y_{S,\ \rm fi} \simeq 3.989 \times 10^{-12} \left(\frac{\lambda_{HS}}{4.48 \times 10^{-12}}\right)^2 , \tag{5.18}$$

$$f_{S,\ \rm fi} \simeq 0.01 \left(\frac{\lambda_{HS}}{4.48 \times 10^{-12}}\right)^2 \left(\frac{m_S}{0.1\ \text{GeV}}\right). \tag{5.19}$$

These results reproduce the abundance in a freeze-in regime by fixing the mass m_S and the coupling λ_{HS}. Nevertheless, it is only valid when λ_{HS} satisfies the condition stated in Eq. 5.17. Hence, this new interaction allows to reproduce the DM abundance for lower values of m_S, as will be seen in Section 6.

5.4 Late decays: $S \to \chi\nu$

The Seesaw model (Sec. 2) of neutrinos leads to a mixing between the mass and flavor eigenstates of the SM neutrinos and the sterile ones.When this mixing is expanded into the Lagrangian, an additional term appears: $\mathcal{L}_{new} = y_S \theta S \bar{\nu} \chi$, as discussed in Section 5.1. If $m_S > m_\chi$, this interaction leads to the decay $S \to \chi\nu$, whose Feynman diagram at tree level is identical to that shown in Figure 6. As in the previous part, we must compute the decay rate $\Gamma(S \to \chi\nu)$, which provides information about the lifetime of the dark scalar τ_S and its contribution to the total dark matter relic abundance. Following the same procedure as in Section 5.2, one finds that the expression for the decay rate is analogous to Eq. B.2, with the replacement $m_N \to m_S$. When it comes to kinematics, assuming that decay is produced with S at rest, the momenta of the decay system are

$$\begin{cases} p_S = (m_N, 0)\,, \\ p_\chi = (E_\chi, \vec{p}_{CM})\,, \\ p_\nu = (E_\nu, -\vec{p}_{CM})\,, \end{cases} \qquad \text{where } |\vec{p}_{CM}| = \frac{m_S}{2}\left(1 - \frac{m_\chi^2}{m_S^2}\right). \tag{5.20}$$

Energy–momentum conservation has been applied, and the small active neutrino mass $m_\nu \sim 0$ has been neclected. Once it has been computed the kinematically part, one have to focus on the scattering amplitude of the process. Following the same Feynman rules as in the N decay, the scattering matrix for two outgoing fermions is now given by $\mathcal{M} = -i y_S \theta \bar{u}(p_\chi)\bar{u}(p_\nu)$, where the interaction vertex has been included. Since S is a scalar particle (spinless), we have that $\overline{|\mathcal{M}|^2} = |\mathcal{M}|^2$. Thus, spin-averaged squared amplitude becomes $\overline{|\mathcal{M}|^2} = 4 y_S^2 \theta^2 p_\chi p_\nu$.

From the definitions of the 4-momenta in Eq.5.20, and using $E_\chi = \sqrt{m_\chi^2 + |\vec{p}_{CM}|^2}$ and $E_\nu = |\vec{p}_{CM}|$, the decay rate becomes

$$\Gamma_{S\to\chi\nu} \equiv \frac{1}{\tau_S} \simeq \frac{y_S^2 m_S}{8\pi}\left(\frac{m_\nu}{m_N}\right)\left(1 - \frac{m_\chi^2}{m_S^2}\right)^2, \tag{5.21}$$

where it has been used the mixing angle $\theta \simeq \sqrt{m_\nu/m_N}$. This expression relates the lifetime τ_S with the mass of the dark sector particles m_S and m_χ, the active and sterile neutrino masses m_ν and m_N, and the Yukawa coupling y_S.

To estimate the temperature at which the decay occurs, we impose that the decay is peaked at a time when $\tau_S \sim 1/H$. By equating both expressions in Eq. 3.2 and 5.21, one fins that the temperature at the moment of the decay $T_{\rm dec}$ is given by

$$T_{\rm dec} \simeq \left(\frac{M_{\rm Pl}}{1.66\ \tau_S \sqrt{g_*(T_{\rm dec})}}\right)^{1/2}. \tag{5.22}$$

Both the lifetime and the decay temperature are of great importance, as they have significant cosmological consequences. The active neutrinos produced in the decay lead to an additional electromagnetic energy injection into the universe, which can impact on its evolution and structure formation. These effects depend strongly on both the energy of the active neutrinos produced in the decay and the epoch at which it occurs. These effects, along with the constraints imposed by observations, are discussed in the following Section 5.5.

5.5 Cosmological constraints

While the landscape of viable candidates is very wide, extensions of the SM often involve feebly interacting massive particles (FIMPs) that possess small couplings to the SM sector. Their inclusion in the primordial plasma comes with potential consequences for fundamental probes of the early Universe, such as primordial Big Bang Nucleosynthesis (BBN) and the comsic

microwave background (CMB). Indeed, just their presence in the system already contributes to the dynamics of the expanding Universe. In particular, decays occurring at the time of the BBN ($\sim$ 1 s) or recombination ($\sim 10^{13}$ s) have implications for the observations. Hence, such scenarios of DM production seen in the previous section are typically constrained by BBN and CMB measurements.

Consequently, any viable physical theory must be consistent with observational data. In particular, cosmological observations place important constraints on the parameter space of theoretical models. These constraints play a crucial role in narrowing down the range of acceptable models, ensuring that theoretical developments remain grounded in empirical reality. Therefore, the compatibility of a model with cosmological data is not just a desirable feature but a fundamental requirement for its physical relevance.

Three relevant constraints must be taken into account for this model (for more detail see Refs. [66, 67, 68]). As discussed in Section 5.4, a new heavy dark scalar particle S undergoes the decay $S \to \chi\nu$, where χ is a FIMP DM candidate and ν is an active neutrino. As will be shown, the smallness of the couplings induces a late decay that can peak around the time of BBN or recombination. Since neutrinos are very weakly coupled, these decays induce an extra electromagnetic energy injection into the thermal bath, commonly known as "electroweak showers", which may affect in various ways both the CMB spectrum and the process of light-element formation during BBN.

Therefore, observations of the evolution and structure formation of the Universe may impose several constraints on the decay, which mainly depends on the effects caused by these newly produced neutrinos ν. On the one hand, in Sections 5.5.1 and 5.5.2 we will focus on both the effects of neutrinos on the spectrum of the CMB and on the light elements formation during the BBN. On the other hand, the introduction of this extra energy density will induce some deviations in the effective number of relativistic species $N_{\rm eff}$, a constraint to be studied on Section 5.5.3.

5.5.1 Cosmic microwave background

The main impact of an energy injection into the CMB photon plasma is given by the inevitable modification it causes to the recombination and reionization evolution. This happens on the one hand, because of the increased photon (and baryon) temperature, which can alter the thermal history of the Universe. On the other hand, the injection of additional high-energy particles can directly reionize the plasma if recombination has already happened. The relative contribution of these effects and their overall impact on the CMB power spectra is mainly dictated by the lifetime of the decaying particle τ_S and by the total amount of energy that is effectively injected in the form of EM radiation.

By taking into account both anisotropies and spectral distortions from CMB, several constraints on the lifetime and the mass must be included in the model. Spectral distortions represent the deviations in the photon distribution induced by energy injection, relative to that of a blackbody spectrum. That is, electroweak showers give rise to a redistribution of photons that can be compared with observations. Consequently, by measuring the deviation from observational data and analyzing the influence of neutrinos produced in the decay, one can derive a set of constraints on the decay time (τ_S) and on the neutrino energy, that can be finally related to m_S.

5.5.2 Big Bang Nucleosynthesis

In order to tighten bounds to even smaller lifetimes, one can also account for constraints from BBN, which describes the process of light element formation in the early Universe, at temperatures $T \sim$ keV - MeV. Any BSM scenario can affect the BBN production in three different ways: (I) by increasing the Hubble rate and thus the expansion rate of the Universe; (II) by altering the time-temperature relation via the injection of EM energy; and (III) by inducing late-time photodisintegration reactions that can destroy the light nuclei previously created during

BBN. That is, the decay products of the produced neutrinos can destroy atoms of the light elements formed, leading to a variation in their abundance.

As the light-element abundances have recently been measured in Refs. [69, 70], more stringent constraints on the decay $S \to \chi\nu$ may be incorporated into the model.

5.5.3 Deviations on the effective number of relativistic species: $\Delta N_{\rm eff}$

By taking into account the extra injection of high-energy neutrinos from the decay, with energy density $\rho_{\rm dark}$, the total radiation density of the Universe can be redefined as $\rho_{\rm rad} = \rho_\gamma + \rho_\nu + \rho_{\rm dark}$. The effective number of relativistic species, $N_{\rm eff}$, is given by

$$N_{\rm eff} = \frac{8}{7}\left(\frac{11}{4}\right)^{4/3}\left(\frac{\rho_{\rm rad}-\rho_\gamma}{\rho_\gamma}\right) = \frac{8}{7}\left(\frac{11}{4}\right)^{4/3}\left(\frac{\rho_\nu}{\rho_\gamma}\right) + \frac{8}{7}\left(\frac{11}{4}\right)^{4/3}\left(\frac{\rho_{\rm dark}}{\rho_\gamma}\right), \tag{5.23}$$

where the first term represents the contribution of the active neutrinos, $N_{\rm eff}^{SM} \simeq 3.044$ and the second one is $\Delta N_{\rm eff}$, which accounts for the correction due the the extra energy injection. Hence, any deviation from the SM prediction provides information about additional relativistic degrees of freedom. $\Delta N_{\rm eff}$ must be computed in order to obtain constraints on both the time decay producing the the electroweak shower (in our model the lifetime τ_S) and the energy of the produced neutrinos (related with m_S). Therefore, to quantify these contributions, one must study how this energy injection affects the effective number of relativistic species $N_{\rm eff}$. By definition, the energy density of neutrinos produced from the decay of S, representing an extra electromagnetic energy injection, can be defined at the time of the CMB as

$$\rho_{\rm dark} = E_\nu(T_{\rm CMB}) n_{\nu_{\rm CMB}}\,. \tag{5.24}$$

Here, since each decay of S produces one ν, one can impose $n_{\nu_{\rm CMB}} = n_{S_{\rm CMB}} = Y_S\ s(T_{\rm CMB})$. The energy of the neutrino at the CMB epoch would be redshifted due to the expansion of the Universe, and can be written as $E_\nu(T_{\rm CMB}) = E_\nu(T_{\rm dec})T_{\rm CMB}/T_{\rm dec}$, where $E_\nu(T_{\rm dec})$ and $T_{\rm dec}$ are computed in Section 5.4. One may finally focus on the relation between $\Delta N_{\rm eff}$ and the lifetime τ_S, which has been computed in Appendix C. Hence, at established by Eq. C.4, we finally arrive to the direct relation

$$\Delta N_{\rm eff} \propto f_S\sqrt{\tau_S}\,, \tag{5.25}$$

where f_S represents the relative dark particle S abundance with respect to Planck observations, while τ_S indicates the lifetime of S.

As represented in Fig 2. from Ref. [67] and in Figure 11 from Ref. [68], the overall BBN, CMB and $\Delta N_{\rm eff}$ constraints lead to a restricted parameter space for the lifetime τ_S and the scalar mass m_S, results that have been implemented in this model. When it comes to $N_{\rm eff}$, the actual experimental bound is given by $\Delta N_{\rm eff} < 0.285$, obtained from Planck Collaboration [71]. Moreover, future sensitivity experiments are expected to obtain $\Delta N_{\rm eff} < 0.06$, by CMB-S4 [72, 73], and $\Delta N_{\rm eff} < 0.028$ by CMB-HD [74].

There is one last constraint that must be taken into account, which establishes a lower bound on the DM particle mass, arising from the impact of warm dark matter (WDM) on the structure formation at small scales. It is known that DM cannot be too relativistic at the time of galaxy formation, as it would have smoothed out anisotropies from the CMB. Hence, constraints on the free-streaming length, provided by Lyman-alpha observations of the 21cm Hydrogen line [75, 76, 77], lead to a bound on the DM mass:

$$m_\chi \gtrsim 1.9\ {\rm keV}\left\langle\frac{p}{T}\right\rangle_d\left(\frac{g_*^{SM}}{g_*(T_d)}\right)^{1/3}, \tag{5.26}$$

where $g_*(T_d)$ represents the number of relativistic degrees of freedom at the moment of χ production, and $\langle\frac{p}{T}\rangle_d$ denotes the average momentum-to-temperature ratio. In the case where the dominant contribution arises from the decay $S \to \chi\nu$, and assuming the decay occurs at $T \sim m_S$, one obtains the bound $m_\chi \gtrsim 5$ keV.

6 Results

After presenting the theoretical model in Section 5, we proceed to analyze the feasible parameter space in order to simultaneously account for three key observables: the origin of neutrino masses, the BAU, and the present-day DM relic abundance. To this end, we study the constraints on the model's free parameters, which include the masses m_χ, m_S, and m_N, together with the couplings y_S, y_ν and λ_{HS}. These parameters govern the relevant dynamics in each sector and determine whether a unified explanation of the observed phenomena can be achieved within this framework. However, the coupling between the sterile neutrinos and the DM, y_S, can be fixed considering that the relic DM abundance is dominated by the cold component from N decays (see Section 5.2). Consequently, all the constraints and conditions derived in Sections 5.2, 5.3, 5.4 and 5.5 enable a thorough exploration of the parameter space in which the model matches the observations.

6.1 Freeze-out production of S

To relate the sterile neutrino mass with the DM one we have to compute the constraints arising from the decay $N \to \chi S$. By tuning the relic dark-matter abundance to the best-fit CDM value reported by the Planck satellite, $\Omega_\chi h^2 = \Omega_{Pl} h^2$ (i.e. $f_\chi = 1$), the relation between m_N and m_χ becomes fixed for each chosen value of the coupling y_S, as follows from Eq. 5.9. As illustrated in Figure 8, every value of y_S defines a distinct set of (m_χ, m_N) pairs that reproduce the relic abundance. In addition, all points in the $m_\chi - m_N$ plane located below the $f_\chi = 1$ curve correspond to an overabundant dark-matter region, that is, the predicted dark matter abundance exceeds the observed one, $\Omega_\chi h^2 > \Omega_{Pl} h^2$. This overabundance leads to a restriction on the viable parameter space as a function of the coupling strength.

The gray region indicates the domain where $m_\chi \gtrsim m_S$, so that S is stable because the decay $S \to \chi\nu$ discussed in Sec. 5.4 is kinematically forbidden. This would lead to a stable dark scalar, an scenario ruled out by direct detection experiments. The hatched region is excluded: if $m_\chi + m_S > m_N$, the decay $N \to \chi S$ will no longer be kinematically allowed, so that N could not decay into DM particles.

On the one hand, in Figure 8 we consider Higgs-portal couplings of order $\lambda_{HS} \sim \mathcal{O}(1)$, so that the production of S particles proceeds via the freeze-out mechanism. In this case, the abundance of S from the FI decay $N \to \chi S$ is washed-out as it is generated out-of-equilibrium, such that the number density n_S is dominated by the freeze-out production. Therefore, the values of m_S and λ_{HS} have been fixed by requiring that the contribution of S to the DM relic abundance, given by Eq. 5.15, is $f_S \simeq 0.01$. One finds that $m_S = 400$ GeV and $\lambda_{HS} = 1$ reproduce the desired relic abundance fraction.

The most notable feature is that, through the introduction of resonant leptogenesis in Section 4.2, the present framework successfully reproduces the observed dark matter abundance, $f_\chi = 1$, for a range of right-handed neutrino masses that are up to six orders of magnitude lower than those required in the original model [1]. Furthermore, we observe that as m_N decreases, the allowed range for the dark matter mass m_χ remains essentially unchanged, whereas the values of the couplings y_S required to reproduce the correct abundance become smaller.

The blue-shaded area at the upper region of the plot indicates the parameter space excluded by BBN and CMB observations. As stated in Section 5.5, several constraints can be introduced into the model arising from the impact of the active neutrinos, produced in the decay $S \to \chi\, \nu$, on cosmic evolution and structure formation in the Universe. As these effects hardly depend on the lifetime τ_S and the mass m_S, once the mass $m_S = 400$ GeV and the relative abundance $f_S \simeq 0.01$ have been fixed, the CMB + BBN constraints can be reproduced for each value of the coupling y_S, which have been extracted from Refs. [67, 68]. This dependence arises primarily because a larger coupling y_S between the dark sector and active neutrinos leads to delayed decays, which in turn impose stronger constraints on the allowed values of the mass of the right-handed

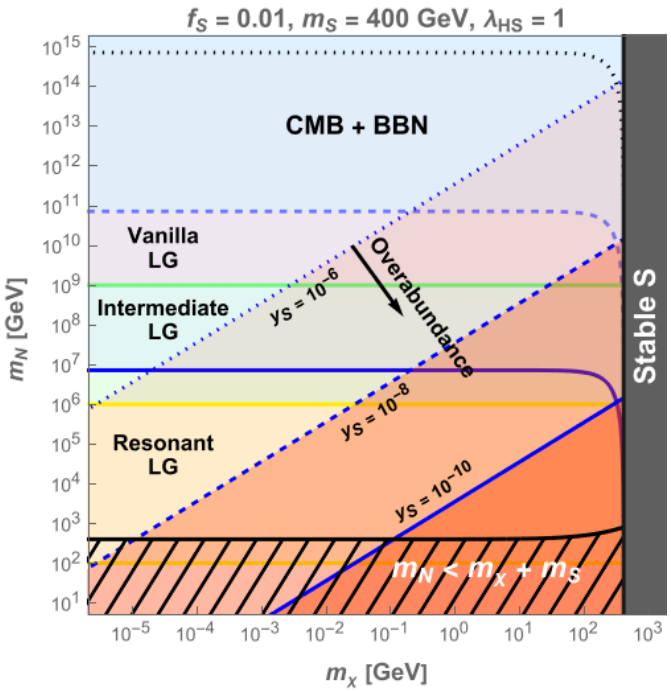

Figure 8: Plane of sterile neutrino and DM masses. We represent the range of sterile neutrino masses m_N valid for each dark matter mass m_χ, with $m_S = 400$ GeV and $\lambda_{HS} = 1$ ($f_S = 0.01$). We show regions of $f_\chi = 1$ for $y_S = 10^{-6}$, 10^{-8} and 10^{-10} in dotted, dashed and solid lines, with its corresponding cosmological constraints. Three different type of leptogenesis are able within this range.

neutrinos.

In this scenario the cold-dark-matter component χ is produced via freeze-in, whereas the dark scalar S is generated through freeze-out. This variant of the model greatly reduces the allowed mass range for the right-handed neutrinos m_N. That is, for lower values of m_N and m_χ we can still reproduce the required abundances $f_\chi \simeq 1$ and $f_S \simeq 0.01$. For each value of the coupling y_S, the viable parameter space is bounded by the restriction $f_\chi \lesssim 1$ (blue solid, dashed and dotted lines represent the abundance $f_\chi = 1$ for $y_S = 10^{-10}$, $y_S = 10^{-8}$ and $y_S = 10^{-6}$), their respective BBN + CMB constraints, and by the kinematically forbidden regions. Consequently, we achieve a lower sterile-neutrino mass scale while still reproducing the BAU and neutrino masses with resonant leptogenesis, up to the lower bound on the dark scalar mass $m_S \gtrsim \frac{m_h}{2} \simeq 62.5$ GeV.

One may wonder now whether freeze-out production of S could succeed when $m_S < m_h$. Although we have not analysed this regime in detail, we can focus on earlier results on the literature. The first consideration we must take into account is that Eq. 5.12 is no longer adequate, but instead we must use the most general expression, which includes not only the annihilation channel $SS^\dagger \to hh$ but also the possible channel $SS^\dagger \to h \to f\bar{f}$, which is kinematically accessible despite the fact that $m_S < m_h$. Taking both contributions into account, the full expression for the thermal annihilation cross-section σv is given by Eq.9.7 of Ref.[39].

This extra term in the cross section leads to a constant relic abundance f_S for low dark scalar masses m_S, because freeze-out is now determined by the annihilation $hh \to SS^\dagger$, as presented in Figure 9.2 of Ref. [39] and Figure 1 from Ref. [78]. Hence, we can think out two possibilities for lower m_S, always in the freeze-out regime: relative large portal couplings $\lambda_{HS} > 10^{-3}$, or lower ones, $\lambda_{HS} < 10^{-3}$.

Large Higgs-portal couplings are excluded by collider detections of $h \to SS$, so reproducing the dark-scalar abundance for $m_S \ll m_h$ is only possible through weak Higgs-portal couplings. As presented in Figure 9.2 of Ref. [39], for each scalar mass m_S, all possible couplings are limited

by an upper bound established by direct detections. Hence, by fixing m_S we can infer which couplings are viable. Within this allowed region, it is possible to reproduce the relic abundance f_S from Eq. 5.15 for different combinations of m_S and λ_{HS} in the viable parameter space.

With this abundance, and using the expression for the lifetime τ_S from Eq. 5.21, we satisfy the conditions required to reproduce the observed value of ΔN_{eff} from Eq. C.4, still assuming that the entire dark-matter density is provided by the dark fermion χ, i.e. $f_\chi = 1$. However, as for the freeze-in production of S, we find out that the entire region that yields the BAU for $m_S < m_h$ is excluded by ΔN_{eff} bounds, as we obtained $\Delta N_{\text{eff}} > 0.285$ for all the parameter space.

We therefore conclude that this scenario of the model where the dark scalar S is produced through the freeze-out mechanism does only account for $m_S > m_h$. Therefore, within this model it is not possible to reproduce neutrino masses, dark matter and the BAU in the regime of leptogenesis via oscillations, that is, we have lowered the sterile neutrino range mass up to a lower bound 63 GeV $\lesssim m_N$.

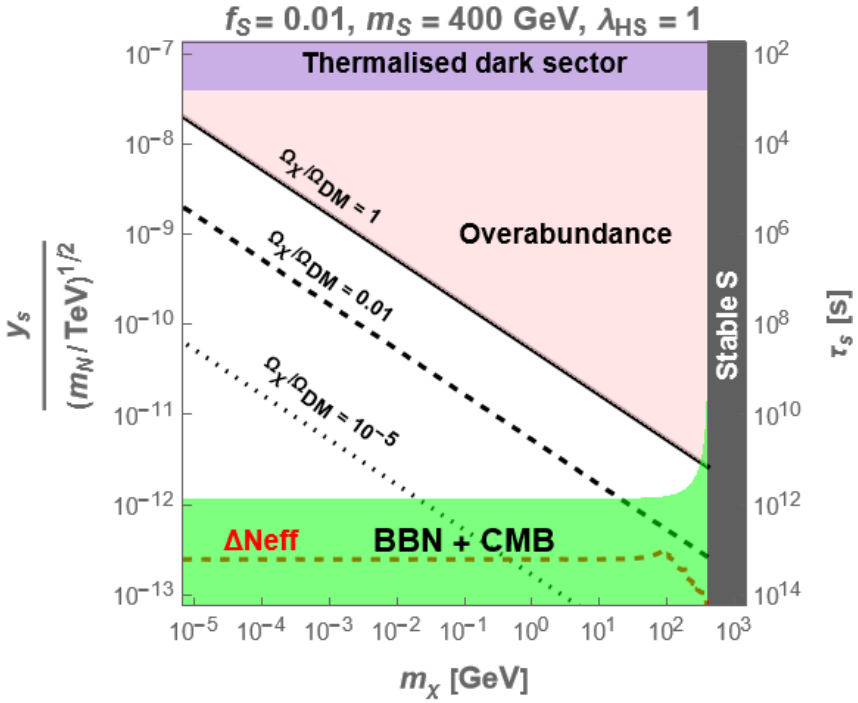

Figure 9: Plane of the DM Yukawa coupling with sterile neutrinos and DM mass, with the lifetime of S on the right axis. We present DM relic abundance fractions $f_\chi = 1,\ 0.01,\ 10^{-5}$ in solid, dashed and dotted lines corresponding to $m_S = 400$ GeV and $\lambda_{HS} = 1$. In green we represent the cosmological constraints on the lifetime.

Secondly, it is well known from Eq. 5.9 that the fraction of the relic DM abundance depends on m_χ, m_S and m_N. Therefore, by fixing the sterile neutrino mass, it is possible to represent different values of the abundance f_χ in the plane $m_\chi - y_S$. More precisely, as $f_\chi \propto y_S^2/m_N$, we can reproduce the most general plot without fixing m_N, as shown in Figure 9. Consequently, if we wish to determine the dark-fermion mass m_χ and the coupling y_S for a a given m_N, we only need to rescale the plot.

In this way, in the plot $y_S/(m_N/\text{TeV})^{1/2}$ as a function of m_χ, we have been able to present the result for different DM abundances: $f_\chi = 1$, $f_\chi = 0.01$ and $f_\chi = 10^{-5}$ are shown as solid, dashed and dotted lines. Hence, if future experiments were to determine the mass of the sterile neutrinos or of the dark-matter particle, we could infer the corresponding coupling required to reproduce the desired relic abundance.

In order to reproduce Figure 9, we consider that the fraction of the relic abundance of the dark scalar produced by the FO mechanism is established at $f_S \simeq 0.01$. Hence, as arises from Eq. 5.15, it order to obtain the desired fraction we fix the values $m_S = 400$ GeV and $\lambda_{HS} = 1$, as done in the previous part. Besides, by taking into account the late decay $S \to \chi\,\nu$ in Section 5.4, one can realize that for a fixed scalar mass $m_S \gg m_\chi$, it is possible to relate directly the lifetime of the dark scalar τ_S with the ratio y_S^2/m_N, as arises from Eq. 5.21. Therefore, in the right-axis of Figure 9 we have represented the corresponding lifetime τ_S for each value of the ratio $y_S/\sqrt{m_N/(\text{TeV})}$.

With respect to Figure 9, four regions are shown that delimit the viable parameter space. On the one hand, the upper excluded region establish that the freeze-in condition in Eq. 5.7 is not satisfied, since for couplings larger than this value the DM particle χ is able to thermalize with the thermal bath, situation that is not compatible with the computation in the FI regime. Moreover, all the parameter space above the plane with $f_\chi = 1$ is not allowed as the predicted dark matter abundance is larger than the observed one, so that $\Omega_\chi > \Omega_{Pl}$ (overabundance).

On the other hand, the introduction of the late decay of S has opened the possibility to represent the corresponding lifetime τ_S in the plot. Hence, for a mixed m_S mass, we are able to present (in green) the bonds given from BBN and CMB observations [67, 68], which excludes larger lifetimes of the dark scalar. Furthermore, it is known that the contribution of active neutrinos produced from the late S decays to the effective number of relativistic species depends on both f_S and τ_S, as arises from Eq. C.4. However, as $f_S \simeq 0.01$ is fixed, the ΔN_{eff} constraint can be reproduced in terms of the lifetime. Therefore, the red-dashed line represent the Planck bound $\Delta N_{\text{eff}} = 0.285$. All the plane above this bound have lower lifetimes, such that all the region is available as $\Delta N_{\text{eff}} < 0.285$, while all the plane above this line is excluded as $\Delta N_{\text{eff}} > 0.285$. Finally, the decay $S \to \chi S$ impose $m_S > m_\chi$, which leads to the kinematically excluded region presented in gray, as for $m\chi > m_S$ the dark scalar should be stable (excluded by direct/indirect detection).

Figure 9 shows that, for a fixed relic dark-matter abundance, for instance $f_\chi = 1$, the ratio $y_S/(m_N/\text{TeV})^{1/2}$ must decrease as larger dark matter masses m_χ are considered. Hence, if m_χ is reduced, one must either lower the coupling y_S or increase the sterile-neutrino mass m_N . In addition, a smaller $y_S/(m_N/\text{TeV})^{1/2}$ ratio, fixed at a given m_S, results in a longer lifetime τ_s, as follows from Eq. 5.4. This generalizes the results obtained in the original model in Ref. [1], which opens up the possibility of exploring the dark-matter abundance for light sterile neutrinos, with masses in the TeV range and below.

Ultimately, by exploiting the mixing between sterile and active neutrinos in Eq. 2.7 and incorporating the most accurate neutrino mass limits $0.01\text{ eV} \lesssim m_\nu \lesssim 0.1$ eV presented by KATRIN experiment [79], it is possible to map the viable parameter space for testable leptogenesis, as comes from Refs. [43, 44, 45]. Moreover, if it is considered the mixing angle for the different flavor eigenstates θ_i, one can define the quantity

$$U^2 \equiv \sum_i |\theta_i|^2\,, \tag{6.1}$$

which quantify the overall mixing between the heavy and light neutrinos. Therefore, once the active neutrino masses are fixed, one can map out the $U^2 - m_N$ plane, as illustrated in Figure 10, plot represented from previous results in Refs. [43, 44, 45, 46].

On the one hand, the lower bounds (black solid lines) are established by fixing the active neutrino mass limits into the mixing angle in Eq. 2.7. Hence, all the intermediate region (blue region) represent the range of values for the mixing angle U^2 and the sterile neutrino mass m_N such that the m_ν is reproduced. The region below this limit is excluded as it reproduces active neutrino masses lower than the bound, $m_\nu < 0.01$ eV. The upper black direct line (purple dotted line) represent the upper limit of the mixing such that the BAU can be reproduced in the freeze-out regime with vanishing (thermal) initial conditions for sterile neutrinos (resonant

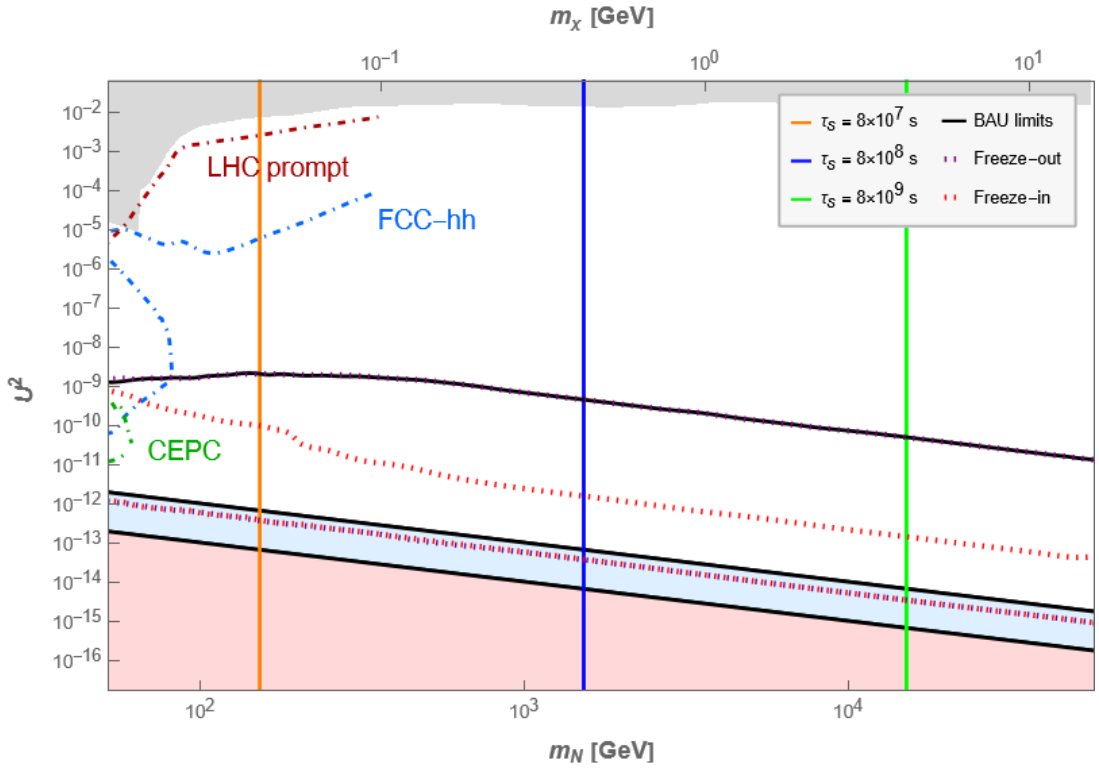

Figure 10: Range of the total mixing angle U^2 consistent with both the seesaw mechanism and leptogenesis as a function of RHNs mass m_N. The solid black line show the results for a vanishing initial abundance of RHNs, while the purple dotted one correspond to thermal initial conditions. The gray area indicates the experimentally excluded region. The dashed-dotted lines represent the estimated sensitivities for actual and future experiments. The upper axis indicates the DM candidate mass m_χ as a function of m_N, under the condition $f_\chi = 1$. The colored solid lines represent different values of the lifetime τ_S of the dark scalar. We have used $m_S = 63$ GeV, $\lambda_{HS} = 0.17$, and $y_S = 10^{-10}$.

leptogenesis). The red, dotted line corresponds to neglecting the effect of the expansion of the Universe on the distribution of the heavy neutrinos, such that the asymmetry is produced during the freeze-in (leptogenesis with oscillations). These results have been already introduced in the literature.

On the other hand, on the upper axis we have introduced the mass of the DM fermion candidate. As presented in the right part of Figure 10, in order to relate the DM mass m_χ with the RHNs one m_N, we have fixed the coupling $y_S = 10^{-10}$ and thus, by imposing $f_\chi = 1$, the corresponding m_χ get fixed for each m_N from the condition given by Eq. 5.9. Moreover, by imposing the condition $f_S = 0.01$ for the lowest achievable dark scalar mass with this model, $m_S = 63$ GeV, Eq. 5.15 leads to a coupling $\lambda_{HS} \simeq 0.17$. With this values, we have been able to reproduce to reproduce several lines for different lifetimes. In such a way, we present in orange, yellow, green and blue the functions corresponding to a lifetime $\tau_S = 8 \times 10^7$ s, 8×10^8 s, 8×10^9 s and 8×10^{10} s. Finally, the colored dashed-dotted lines represent the estimated sensitivities for actual and future experiments whose main objective is the detection of physics beyond the Standard Model.

The main feature of this model is that, by assuming that the total DM abundance is given by this cold DM candidate χ, it predicts the possible DM mass m_χ for each m_N. Therefore, if any future experiment detects these theoretical right-handed neutrinos and measure their mass, within this model we will be able to predict the mass of the DM particle, as well as estimate the lifetime of the proposed dark scalar.

6.2 Freeze-in production of S

In this section, we have considered the case in which the coupling λ_{HS} is not strong enough to allow for thermalization between S and the SM thermal bath. Whenever λ_{HS} satisfies the condition given by 5.17 for a given m_S, the production of S particles proceeds through the freeze-in mechanism, that is, an additional S component is then generated via the decay $h \to SS$. The result for this framework within the Type I seesaw mechanism is presented in Figure 11.

As long as the coupling y_S satisfies the FI condition given by Eq. 5.7, the decay $N \to \chi S$ is still effective. Hence, unlike in the freeze-out case, this contribution to the abundance of S is not washed out, so the relic density of the dark scalar receives one extra component. For every dark fermion χ produced in the decay, one dark scalar S is produced, such that the ratio for the relic abundance for S is thus given by Eq. 5.9 with the interchange $m_\chi \to m_S$. Specifically, the relative abundance $f_{S,\ N\to\chi S}$ can be related to the dark matter abundance f_χ produced by this decay as

$$f_{S,\ N\to\chi S} = \frac{m_S}{m_\chi} f_\chi \,. \tag{6.2}$$

One may realize that, as it has been considered $m_S > m_\chi$, the relic abundance of the scalar S will always be larger than that of the fermion χ, that is, $f_{S,\ N\to\chi S} > f_\chi$. Furthermore, taking into account that the dark scalar population is now given by the contribution of both decays $N \to \chi S$ and $h \to SS$, the total S relic abundance, relative to the best-fit Planck value, is given by

$$f_S = f_{S,\ N\to\chi S} + f_{S,\ h\to SS} \,, \tag{6.3}$$

where $f_{S,\ h\to SS}$ is given by Eq. 5.19. This abundance depends on the free parameters of the theory m_S, m_N, y_S and λ_{HS}. Nonetheless, for a fixed scalar mass m_S, i.e. $m_S = 0.1$ GeV, we can impose an upper bound to λ_{HS}, as arises from Eq. 5.17. In the same way, an upper bound can be established for y_S by requiring that the FI condition stated in Eq. 5.7 is always satisfied throughout the entire range of possible m_N masses shown in Figure 11.

With a fixed mass m_S, the total abundance f_S can be expand in terms of only two parameters, m_χ and m_N. Moreover, as we always fix that the total observed dark matter abundance is given by the abundance of χ, that is $f_\chi \simeq 1$, a several relation between m_N and m_χ arises for each coupling (see Eq. 5.9). Red, blue and green dotted lines represent the set of points $m_N - m_\chi$ that reproduce the abundance $\Omega_\chi h^2 = \Omega_{\rm Pl} h^2$ for $y_S = 10^{-6}$, $y_S = 10^{-8}$ and $y_S = 10^{-10}$ respectively.

Under this condition, each point in the plot yields a specific value of the total relic abundance f_S for every coupling y_S. This value is obtained by taking into account both contributions given by Eqs. 5.19 and 6.2. Hence, by reproducing numerically the solutions for f_S in each point of the parameter space, we realized that it was always much larger than the expected.

Although for $m_S = 0.1$ GeV the combined CMB+BBN observations do not constrain the scalar-lifetime range (see Refs. [67, 68] for further detail), several constraints from $\Delta N_{\rm eff}$ can be inferred from Eq. C.4, where it is represented the dependence on the relic abundance f_S and the lifetime τ_S. The lifetime is given by Eq. 5.21, while f_S can be computed by fixing the dark scalar mass m_S and the Higgs-portal coupling λ_{HS}. Since f_S were too large throughout the entire dark-fermion mass range $m\chi$, we obtained that the predicted value of $\Delta N_{\rm eff}$ exceeds the observational limit every point in the parameter space, $\Delta N_{\rm eff} > 0.285$. Hence, the whole range for low sterile neutrino masses has been excluded. In other words, this model is unable to reproduce the DM abundance through an scenario with freeze-in production of S.

However, one may wonder what would happen to the viable parameter space with the introduction of larger mixing angles arising from the inverse seesaw seen in Section 2.2. The introduction of a new singlet s_L with a Majorana mass term μ introduces the possibility of enlarging the possible mixing angle between active and sterile neutrinos. Therefore, as arises from Eq. 5.21, a larger mixing θ^2 leads to a shorter lifetime τ_S. Hence, as $\Delta N_{\rm eff} \propto f_S\sqrt{\tau_S}$, despite the fact that f_S is very large for the freeze-in production of S, if we reduce the lifetime it will

be possible to reproduce a region of the parameter space which is not excluded by the $\Delta N_{\rm eff}$ constraint, that is, $\Delta N_{\rm eff} < 0.285$.

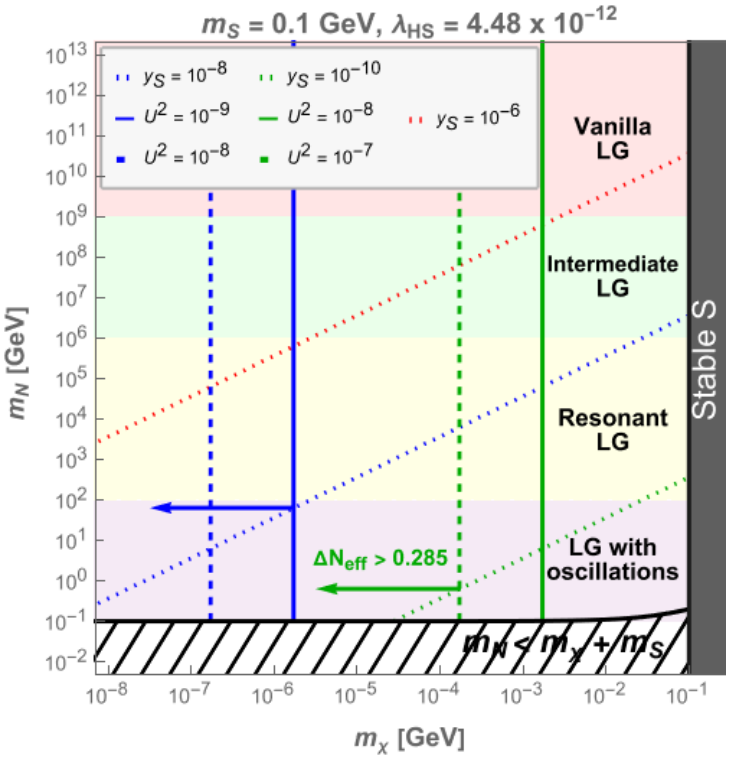

Figure 11: Plane of sterile neutrino and DM masses. We represent the range of sterile neutrino masses m_N valid for each dark matter mass m_χ, with $m_S = 0.1$ GeV and $\lambda_{HS} = 4.48 \times 10^{-12}$. We show regions of $f_\chi = 1$ for $y_S = 10^{-6}$, $y_S = 10^{-8}$ and $y_S = 10^{-10}$ in red, blue and green dotted lines. For each coupling, we represent the limit $\Delta N_{\rm eff} = 0.285$ for different mixing angles: $U^2 = 10^{-9}$, 10^{-8} and $U^2 = 10^{-8}$, 10^{-7}. All the parameter space at the left part of the limits (blue and green solid/dashed lines) is excluded. For the Yukawa coupling $y_S = 10^{-6}$ there is no excluded region.

Therefore, as the inverse seesaw opens up the possibility for larger mixing angles than those corresponding to the Type I seesaw mechanism (blue region from Fig. 1), we have been able to represent in direct and dashed blue (green) lines the bound $\Delta N_{\rm eff} = 0.285$ for the coupling $y_S = 10^{-8}$ ($y_S = 10^{-10}$) with mixings $U^2 = 10^{-9}$ ($U^2 = 10^{-8}$) and $U^2 = 10^{-8}$ ($U^2 = 10^{-7}$) respectively. However, for $y_S = 10^{-6}$ there is no excluded region, as $\Delta N_{\rm eff} < 0.285$ for all the range of DM mass. Notice that neutrino masses are reproduced for this mixings for a given value of the Majorana mass μ.

As indicated in the plot, all the parameter space at the left side of the limits (lower m_χ) is excluded by the $\Delta N_{\rm eff}$ constraints. As we can see, a larger Yukawa coupling y_S and a larger mixture between active and sterile neutrinos leads to a a lower lifetime τ_S, and therefore a lower value of $\Delta N_{\rm eff}$. Hence, it will be a larger available parameter space, leading to the possibility for lowering the mass range for the sterile neutrinos up to $m_N \gtrsim 0.1$ GeV, depending on the value of the Yukawa coupling y_S and the total mixing angle U^2. However, we can see that the bounds on $\Delta N_{\rm eff}$ does not depend on m_N as the lifetime does only depends on the coupling y_S and the mixing, while the Yukawa coupling for neutrinos, $y_\nu = \theta\, m_N/v$, vary significantly along the vertical lines.

Hence, we have seen that the larger mixing angles available via the inverse seesaw lead to the possibility of lighter sterile neutrino and dark matter masses for the freeze-in production of S, as large fractions f_S are offset by the short lifetimes τ_S, leading to $\Delta N_{\rm eff}$ values that remain allowed

throughout the entire parameter space. Consequently, introducing the inverse-seesaw mechanism opens the possibility to analyzing the model for sterile neutrino masses in the vicinity of the GeV scale.

7 Conclusions

The SM can not simultaneously account for neutrino masses, the baryon asymmetry of the Universe and dark matter within a single coherent framework. It is therefore interesting to consider a framework that may address all these issues: The seesaw leptogenesis paradigm is one of the best-motivated extensions of the SM to address neutrino masses and the BAU, but it does not account for the origin and composition of dark matter. By introducing an additional dark sector, our proposed model seeks to establish a unified, testable framework that overcomes all of these shortcomings of the SM at once.

Within this model, we have introduced a dark fermion χ, considered to be the dark matter candidate, and a dark scalar S. We considered that both dark particles χ and S can couple to right-handed neutrinos N. Furthermore, the presence of S and its Higgs-portal interactions opens up the possibility to different type of interactions. That is, the introduction of S makes the physics of the DM candidate χ very rich.

The dark fermion χ is mainly produced through the freeze-in mechanism, such that very small Yukawa couplings are required. However, for the dark scalar S we consider two distinct production channels: via freeze-out annihilations $SS^\dagger \to hh$ and through freeze-in decays $h \to SS$.

On the one hand, through the FO production of S, we reproduce the results obtained in the original model [1]. Moreover, with this low-scale analysis we have been able to reproduce the dark matter abundance, neutrino masses and the BAU in the resonant leptogenesis regime. In such a way, we have lowered the right-handed neutrino mass scale by up to six orders of magnitude compared to the original model, up to a lower bound 63 GeV $\lesssim m_N$. Therefore, we can conclude that this model successfully reproduces the dark-matter abundance at a low right-handed-neutrino mass scale, provided that the dark scalar S is generated through freeze-out.

Furthermore, one of the most compelling features of this model is that the dark-matter abundance is inversely proportional to the sterile-neutrino mass m_N and directly proportional to the dark-fermion mass m_χ, that is, $f_\chi \propto m_\chi/m_N$. Hence, the model yields a correlated prediction for m_χ and for the lifetime of the dark scalar τ_S at each value of right handed neutrino mass. Should future new-physics experiments succeed in detecting right-handed neutrinos, the model would then provide a concrete theoretical estimate for the corresponding dark-matter mass.

On the other hand, we have been able to analyze the model under the freeze-in production of S from the decay $h \to SS$. After studying the model and analyzing the viable parameter space, we realized that as there is no freeze-out production that washes out the abundance of S arising from the decay $N \to \chi S$, the predicted fraction of the relic abundance f_S is too large for all the considered mass range. Therefore, this large relic abundances leads to several constraints on the ΔN_{eff} of this model, where we obtain that all the parameter space is excluded as $\Delta N_{\text{eff}} > 0.285$. Hence, we can conclude that this model does not account for an scenario where the dark scalar abundance is produced through the freeze-in mechanism.

However, through the introduction of the inverse seesaw mechanism, we realized that the large available mixing angles between active and sterile neutrinos leads to shorter lifetimes. Hence, these shorter lifetimes compensate the large fractions of the relic abundance f_S produced by the freeze-in mechanism, leading to a region of the parameter space whose values of ΔN_{eff} are not excluded constraints. Therefore, depending of the value of the Yukawa coupling y_S and the total mixing U^2, it is possible to reduce the range of sterile neutrinos up to 0.1 GeV $\lesssim m_N$.

To sum up, the results obtained within this model can be summarized as follows: as long as the dark scalar S abundance is produced through freeze-out (annihilation $SS^\dagger \to hh$) mechanisms,

the model furnishes a testable scenario that unifies neutrino masses, the matter–antimatter asymmetry and the dark-matter abundance within a single theoretical framework. In this work, we further checked that low masses for the sterile neutrino, as low as 63 GeV, are possible. Moreover, the introduction of the inverse seesaw leads to the possibility of reducing the range of the right-handed neutrino mass up to 0.1 GeV.

A thorough future study of the inverse seesaw and its impact on leptogenesis could provide a more precise and systematic analysis of the model's effective parameter space, such that this could be the focus of forthcoming work. Another possible future line of investigation involves the regime $m_S > m_N$, which opens the three-body decay $N \to \chi\chi\nu$, with the dark scalar S as a virtual propagator.

A Boltzmann equations

It is well known that, for much of its early history, most of the constituents of the Universe were in thermal equilibrium, thereby making an equilibrium description a good approximation. However, because the Universe expands at a rate H, once the interaction rate of a particle falls below the expansion rate, the different species decouple from the primordial plasma, leading to the relic abundance that can be detected today. Hence, given a particle P, if $\Gamma_P \gtrsim H(T)$, the particle can be considered to be thermally coupled to the Universe plasma, whereas if $\Gamma_P < H$, the particle decouples from the plasma and no longer interacts with it, leading a "frozen" abundance.

At this point, in order to treat decoupling, one must follow the microscopic evolution of the particle's phase-space distribution function $f(p^\mu, x^\mu)$, which is governed by the Boltzmann equation, introduced in 1872 by Ludwig Boltzmann [80], and reads as

$$\hat{L}[f] = C[f]\,. \tag{A.1}$$

In this equation, $\hat{L}$ represents the Liouville operator, while C denotes the collision term for each particle species. This collision term is usually expressed in terms of the squared amplitude matrix of the process, $|\mathcal{M}|^2$, and the available phase space. The relativistic Liouville operator can generally be written as

$$\hat{L} = p_\alpha \frac{\partial}{\partial x_\alpha} - \Gamma^\alpha_{\beta\gamma}\, p^\beta p^\gamma \frac{\partial}{\partial p_\alpha}\,. \tag{A.2}$$

Both parts of the equation can now be integrated and, after adding the appropriate factors for the Robertson–Walker metric, it gives

$$\frac{g}{(2\pi)^3}\int d^3p \left(\frac{\partial f}{\partial t} - Hp\frac{\partial f}{\partial p}\right) = \frac{g}{(2\pi)^3}\int d^3p\, \frac{C[f]}{E}\,. \tag{A.3}$$

Using the definition of the number density,

$$n(t) = \frac{g}{(2\pi)^3}\int d^3p\, f(E,t)\,, \tag{A.4}$$

the first term of the left-hand equation is $dn(t)/dt$. The second term can be computed from integration by parts. Let's consider a Boltzmann distribution function $f(p) \propto e^{-p/T}$, where $p \equiv |\vec{p}|$ indicates the tri-momentum of the particle. For a FRW universe, one can expand $d^3p = 4\pi p^2 dp$, such that the second term becomes

$$-H\frac{g}{(2\pi)^3}\int_0^\infty 4\pi p^3 dp \frac{\partial f}{\partial p} = -4\pi H \frac{g}{(2\pi)^3}\left[\cancel{f(p)p^3\Big|_0^\infty} - 3\int_0^\infty f(p)p^2 dp\right] = 3Hn(t)\,, \tag{A.5}$$

where the term $f(p)p^3\Big|_0^\infty$ has been canceled as $f(p)$ tends to 0 fast enough when p goes to ∞. Therefore, the momentum-integrated Boltzmann equation becomes

$$\frac{dn}{dt} + 3Hn = \frac{g}{(2\pi)^3}\int \frac{d^3p}{E}\, C[f]\,, \tag{A.6}$$

where $H = \dot{a}/a$ denotes the Hubble expansion rate. Since the Liouville operator in curved space-time is modified by the expansion when the metric is isotropic and homogeneous (FRW), the collision term $C[f]$ must be evaluated in order to solve these Boltzmann equations (BEs) numerically. Their solutions provide the time evolution of the comoving number density, $Y \equiv n_\psi/s$. The following sections focus on solving the BE for both mechanisms of interest: In Appendix A.1, we solve the BEs for the freeze-out mechanism, while in Appendix A.2 they have been solved in the freeze-in regime.

A.1 Freeze-out

One objective is to compute the collision term for each process, whose general expression is given by Eq. (5.8) of [27]. Under this prescription, the Boltzmann equation reads

$$\begin{aligned} \dot{n}_S + 3Hn_S = \int d\Pi_S\, d\Pi_{S^\dagger}\, d\Pi_H\, d\Pi_{H^\dagger}\, (2\pi)^4 \delta^4\big(p_S + p_{S^\dagger} - p_H - p_{H^\dagger}\big) \\ \times \Big[|\mathcal{M}|^2_{HH^\dagger \to SS^\dagger} f_H f_{H^\dagger} (1 \pm f_S)(1 \pm f_{S^\dagger}) - |\mathcal{M}|^2_{SS^\dagger \to HH^\dagger} f_S f_{S^\dagger} (1 \pm f_H)(1 \pm f_{H^\dagger}) \Big] , \end{aligned} \tag{A.7}$$

where f_i denotes the distribution function of particle i; the sign + (−) applies to a bosonic (fermionic) final states. The differential phase space is defined as

$$d\Pi_i \equiv \frac{g_i}{(2\pi)^3} \frac{d^3 p_i}{2E_i} , \tag{A.8}$$

where g counts the integral degrees of freedom, and E the energy of the particle. Solving the Boltzmann equation therefore requires evaluating the squared scattering amplitude $|\mathcal{M}|^2$, and integrate it over phase space.

At this stage, and in the absence of Bose condensation or Fermi degeneracy, the stimulated-emission factors can be neglected, $(1 \pm f_i) \simeq 1$. Assuming further that kinetic equilibrium holds between the initial and final states owing to faster scattering processes, the distribution functions can be written as

$$f_i(p) = \frac{n_i}{n_{i,\mathrm{eq}}}\, e^{-E_i/T} . \tag{A.9}$$

We can assume now that there is no CP violation, such that $|\mathcal{M}|^2_{SS^\dagger \to HH^\dagger} = |\mathcal{M}|^2_{HH^\dagger \to SS^\dagger} \equiv |\mathcal{M}|^2$ and $n_S = n_{S^\dagger}$, $n_H = n_{H^\dagger} = n_{H,\mathrm{eq}}$. Hence, imposing detailed balance, $n_h^2 \sigma_{HH^\dagger \to SS^\dagger} = n_S^2 \sigma_{SS^\dagger \to HH^\dagger}$, we can expand the Boltzmann equation in terms of n_S as

$$\dot{n}_S + 3Hn_S = \langle \sigma v \rangle \big[n^2_{S,\mathrm{eq}} - n_S^2 \big] , \tag{A.10}$$

where $\langle \sigma v \rangle$ is defined as in Eq. (5.23) of Ref. [27], or more precisely by Eq. (3.8) from Ref. [81],

$$\langle \sigma_{SS^\dagger \to HH^\dagger} v \rangle \equiv n^{-2}_{S,eq} \int d\Pi_S\, d\Pi_{S^\dagger}\, d\Pi_H\, d\Pi_{H^\dagger}\, (2\pi)^4 \delta^4\big(p_S + p_{S^\dagger} - p_H - p_{H^\dagger}\big) |\mathcal{M}|^2 e^{-(E_S + E_{S^\dagger})/T} . \tag{A.11}$$

Finally, the equation can be rewritten in terms of $Y_S = n_S/s$ and $z = m_N/T$. This can be done by expanding

$$\frac{dn_S}{dt} = \frac{dn_s}{dY_s} \frac{dY_S}{dz} \frac{dz}{dT} \frac{dT}{dt} , \tag{A.12}$$

where the new variable to expand the BE is dY_S/dz, while $dn_s/dY_s = s$, $dz/dT = -m_N/T^2$, and dT/dt can be computed from applying the entropy conservation in an expanding Universe. Using this result, Eq. A.10 can be rewritten as

$$\frac{dY_S}{dz} = \frac{s \langle \sigma v \rangle}{zH} \big[Y^2_{S,\mathrm{eq}} - Y_S^2 \big] , \tag{A.13}$$

where $Y_{S,\mathrm{eq}} = n_{S,\mathrm{eq}}/s$.

A.2 Freeze-in

Following the same procedure used for the freeze-out mechanism. Under the assumptions of no CP violation, negligible stimulated-emission factors, and N and S in equilibrium ($n_N = n_{N,\text{eq}}$ and $n_S = n_{S,\text{eq}}$), the collision term for the decay $N \to \chi S$ is

$$\dot{n}_\chi + 3Hn_\chi = \int d\Pi_S \, d\Pi_\chi \, d\Pi_N \, (2\pi)^4 \delta^4(p_N - p_S - p_\chi) \, |\mathcal{M}|^2 \big(f_N - f_\chi f_S\big) \, . \tag{A.14}$$

At this point, the Boltzmann equation can be written in terms of the decay rate $\Gamma_{N\to\chi S}$, whose expression (in terms of the scattering amplitude and phase space) is obtained by integrating Eq. 5.6 and replacing $m_N \to E_N$ to remain in the most general case. Therefore, we can rewrite the Boltzmann equation as

$$\dot{n}_\chi + 3Hn_\chi = n_N \langle \Gamma_{N\to\chi S} \rangle \Big(\frac{n_N}{n_{N,eq}} - \frac{n_\chi}{n_{\chi,eq}} \frac{n_S}{n_{S,eq}} \Big) \, , \tag{A.15}$$

where the thermal average of the decay rate is

$$\langle \Gamma_{N\to\chi S} \rangle = \frac{\displaystyle\int \frac{d^3p_N}{(2\pi)^3} \, \Gamma \, g_N \, e^{-E_N/T}}{\displaystyle\int \frac{d^3p_N}{(2\pi)^3} e^{-E_N/T}} = \frac{g_N \displaystyle\int \frac{d^3p_N}{(2\pi)^3} \, \Gamma \, e^{-E_N/T}}{n_{N,\text{eq}}} = \frac{K_1(m_N/T)}{K_2(m_N/T)} \Gamma_{N\to\chi S} \, . \tag{A.16}$$

The definition of $n_{N,\text{eq}}$ in Eq. 3.1 has been used and the integral has been expressed with modified Bessel functions $K_n(z) = \frac{1}{2}\big(\frac{z}{2}\big)^n \int_0^\infty t^{-(n+1)} e^{-t - z^2/4t} \, dt$. With these definitions, and assuming N and S are in equilibrium, $n_N = n_{N,eq}$ and $n_S = n_{S,eq}$, the BE becomes

$$\dot{n}_\chi + 3Hn_\chi = n_{N,\text{eq}} \, \frac{K_1(z)}{K_2(z)} \, \Gamma_{N\to\chi S} \Big(1 - \tfrac{n_\chi}{n_{\chi,\text{eq}}} \Big) \, . \tag{A.17}$$

Analogously to the freeze-out regime, it is convenient to rewrite the Boltzmann equation in terms of $Y_\chi = n_\chi/s$ in order to study its evolution, which is related to the relic dark-matter abundance. Thus, the evolution of Y_χ in terms of $z = m_N/T$ is given by

$$\frac{dY_\chi}{dz} = \frac{Y_{N,eq}}{Hz} \frac{K_1(z)}{K_2(z)} \Gamma_N \left[1 - \frac{Y_\chi}{Y_{\chi,eq}} \right] . \tag{A.18}$$

The solutions to equations A.13 and A.18 have been represented in Figures 2 and 3.

B Dark matter production for our model

This appendix presents the theoretical procedures used for the analytical computation of the relative dark matter abundances through different production mechanisms. In Appendix B.1, we study the production of χ particles in the freeze-in scenario, whose development can be reused for the calculation of the abundance of S under the same conditions. Finally, in Appendix B.2, we examine the theoretical framework for computing the production of S in the freeze-out regime.

B.1 Freeze-in production of χ

In this section, we are interested on computing the decay rate given by the process in Figure 6. The starting point should be the differential form of the decay rate, given by Eq. 5.6.Then,

one may compute kinematics for the decay. Considering N in the rest frame, the momenta of the particles can be defined as

$$\begin{cases} p_N = (m_N, 0) \\ p_\chi = (E_\chi, \vec{p}_{CM}) \\ p_S = (E_S, -\vec{p}_{CM}) \,. \end{cases} \quad \text{where } |\vec{p}_{CM}| = \frac{m_N}{2}\sqrt{1-\left(\frac{m_\chi+m_S}{m_N}\right)^2}\sqrt{1-\left(\frac{m_\chi-m_S}{m_N}\right)^2} \tag{B.1}$$

By integrating over the phase space d^3p_χ and d^3p_S the 4-momentum conservation, one can finally arrive to

$$\Gamma(N \to \chi S) = \frac{|\vec{p}_{CM}|}{8\pi m_N^2}\overline{|\mathcal{M}|^2}\,, \tag{B.2}$$

so the problem has been reduced to compute the reduced scattering amplitude for this decay. Taking into account the sum over initial spinors, $\overline{|\mathcal{M}|^2} = \frac{1}{2}|\mathcal{M}|^2$, which can be computed by applying the corresponding Feynman rules. For an incoming fermion with momenta p_N and an outgoing fermion with p_χ, the matrix element is given by $\mathcal{M} = -iy_S u(p_N)\bar{u}(p_\chi)$, where $-iy_S$ represents the contribution of the vertex, leading to

$$|\mathcal{M}|^2 = \mathcal{M}\mathcal{M}^\dagger = y_S^2 Tr[(\not{p}_N + m_N)(\not{p}_\chi + m_\chi)] = y_S^2(p_N p_\chi + m_N m_\chi)\,, \tag{B.3}$$

where properties of the gamma matrices have been used up. Using that $p_N p_\chi = m_N E\chi$, where $E_\chi = \sqrt{m_\chi^2 + |\vec{p}_{CM}|^2}$, and considering $m_N \gg m_\chi$, one can finally arrive to

$$\Gamma(N \to \chi S) \simeq \frac{y_S^2}{16\pi} m_N\,. \tag{B.4}$$

On the one hand, the freeze-in condition to the coupling arises from imposing $\Gamma < H$. Using the expression for the Hubble rate from Eq. 3.2, and considering that the production rate peaks at $T_{\rm fi} \sim m_N/3$, the upper bound for the Yukawa coupling such that the DM particle do not thermalize is given by

$$y_S^2 \lesssim \frac{16\pi^2}{27}\sqrt{\frac{g_*(T_{\rm fi})}{10}}\frac{m_N}{M_{\rm Pl}}\,. \tag{B.5}$$

On the other hand, as known from Ref. [63], the decay rate can be related with Y_χ as

$$Y_\chi \equiv \frac{n_\chi}{s} \simeq \frac{135 g_N}{8\pi^3 \cdot 1.66 g_{*S}(T_{\rm fi})\sqrt{g_{*\rho}(T_{\rm fi})}}\frac{M_{\rm Pl}\Gamma_{N\to\chi S}}{m_N^2} \simeq \frac{135 g_N M_{\rm Pl}}{128\pi^4 \cdot 1.66 g_{*S}(T_{\rm fi})\sqrt{g_{*\rho}(T_{\rm fi})}}\frac{y_S^2}{m_N}\,, \tag{B.6}$$

the relic dark matter abundance fraction is obtained via Eq. 3.7, leading to a direct relation between m_N, m_χ and y_S,

$$f_\chi \equiv \frac{\Omega_\chi h^2}{\Omega_{Pl} h^2} = \frac{m_\chi\, Y_\chi}{T_{\rm eq}} \simeq \frac{135 g_N M_{\rm Pl}}{128\pi^4 \cdot 1.66\; T_{\rm eq}\; g_{*S}(T_{\rm fi})\sqrt{g_{*\rho}(T_{\rm fi})}}\frac{y_S^2 m\chi}{m_N}\,. \tag{B.7}$$

In order to reproduce numerically the solutions it has been used $g_N = 2$ (effective degrees of freedom of RHNs) and $g_{*\rho}(T_{\rm fi}) = g_{*S}(T_{\rm fi}) \simeq 106.75$, $T_{\rm eq} \simeq 0.4 \times 10^{-9}$ GeV and $M_{\rm Pl} \simeq 1.22 \times 10^{19}$ GeV.

B.2 Freeze-out production of S

On this Appendix, we are interested on computing the interaction rate of the scattering $SS^\dagger \to hh$ in the FO regime. Therefore, we must focus on solving the differential cross section in

Eq. 5.11. Once it is defined, one may focus firstly on the kinematics of the system. Considering the system is on the center-of-mass frame, kinematics leads to:

$$\begin{cases} |\vec{p_1}| = |\vec{p_2}| = |\vec{p_s}| \Rightarrow s = (E_1 + E_2)^2 = 4E_s^2;\ E_s^2 = |\vec{p_s}|^2 + m_s^2\,, \\ |\vec{p_3}| = |\vec{p_4}| = |\vec{p_h}| \Rightarrow s = (E_3 + E_4)^2 = 4E_h^2;\ E_h^2 = |\vec{p_h}|^2 + m_h^2\,. \end{cases} \tag{B.8}$$

Under this conditions, it can be defined the flux factor for a linear collision as

$$I = E_1 E_2 \sqrt{(v_1 - v_2)^2 - (v_1 \times v_2)^2} = E_s^2 v_{rel}\,, \tag{B.9}$$

where v_{rel} represent the relative velocity between the two particles that scatters. On the other hand, in the CM frame it can be rewritten as

$$I = |\vec{p_s}|\sqrt{s} \Rightarrow v_{rel} = \frac{|\vec{p_s}|\sqrt{s}}{E_s^2} = 2\sqrt{1 - \frac{4m_s^2}{s}}\,. \tag{B.10}$$

With these expressions the differential scattering cross section from Eq. 5.11 can be derived in the center-of-mass frame, leading to

$$d\sigma = \frac{1}{32\pi^2 s}|\mathcal{M}_{fi}|^2 \frac{|\vec{p_h}|}{|\vec{p_s}|} d\Omega\,, \tag{B.11}$$

where must be computed the scattering matrix squared $|\mathcal{M}_{fi}|^2$ for this process. From Figure 7, the scattering matrix $\mathcal{M}_{fi}$ is given by the single point-like Feynman vertex, whose contribution is $-i\lambda_{HS}/2$. Taking into account possible combinations of the final states, an extra factor 2 must be introduced to the vertex. With this, the scattering matrix squared becomes $|\mathcal{M}_{fi}|^2 = |\lambda_{HS}|^2$.

From kinematics in the CM frame, since $p_3 = (E_h, \vec{p_h})$ and $p_4 = (E_h, -\vec{p_h})$, the momenta conservation leads to

$$|\vec{p_h}| = \frac{1}{2\sqrt{s}}\sqrt{s^2 - 4sm_h^2} = \frac{\sqrt{s}}{2}\sqrt{1 - \frac{4m_h^2}{s}}\,, \tag{B.12}$$

and then, as an isotropic coupling does not lead to any angular dependence, the scattering cross section becomes

$$\sigma = \frac{|\lambda_{HS}|^2}{32\pi} \frac{1}{\sqrt{s}|\vec{p_s}|}\sqrt{1 - \frac{4m_h^2}{s}}\,. \tag{B.13}$$

Under the assumption $m_s > m_h$, the scattering can be studied in the case where S is in the rest frame, so $|\vec{p_s}| = 0$. In this case, $E_s^2 = m_s^2$ and then $s = 4m_s^2$, such that by introducing Eq. B.10, one obtains

$$\sigma v_{rel} = \frac{|\lambda_{HS}|^2}{64\pi m_s^2}\sqrt{1 - \frac{m_h^2}{m_s^2}}\,. \tag{B.14}$$

Finally, one may compute the number density of dark matter at the present time, $Y_{S,\infty} = n_\chi/s\,|_{fo}$. In order to study the final relic density it must be computed the time of the freeze-out which, as discussed in Section 3.1, corresponds to the time where $\Gamma \simeq H$. On the one hand, the annihilation rate is proportional to $\Gamma \sim n_\chi \langle\sigma v_{rel}\rangle = sY_{S,\infty}\langle\sigma v_{rel}\rangle$, where the number density of the dark matter at the moment of the freezing-out is given by Eq. 3.1, at the regime $T \ll m_\chi$. On the other hand, it is known that the entropy at the early Universe can be expressed in terms of the temperature and the effective number of degrees of freedom as

$$s(T) = \frac{2\pi^2}{45} g_{*s}(T) T^3\,. \tag{B.15}$$

Then, equating the expression for the annihilation rate to the Hubble parameter from Eq. 3.2 at the time of FO,

$$\frac{2\pi^2}{45} g_{*s}(T_{\rm fo}) T_{\rm fo}^3 Y_{S,\infty} < \sigma v_{rel} >= \frac{\pi}{3}\sqrt{\frac{g_*(T_{\rm fo})}{10}} \frac{T_{\rm fo}^2}{M_{\rm Pl}}\,, \tag{B.16}$$

which leads to

$$Y_{S,\infty} \simeq 150\sqrt{10}\pi^2 \sqrt{\frac{g_*(T_{\rm fo})}{g_{*S}^2(T_{\rm fo})}} \frac{m_S}{M_{\rm Pl}|\lambda_{HS}|^2} \left(1 - \frac{m_h^2}{m_S^2}\right)^{-1/2} . \tag{B.17}$$

Once it has been obtained $Y_{S,\infty}$, the relic abundance can be determined from Eq. 3.7 for S and using $T_{\rm fo} \sim m_S/20$,

$$f_S \equiv \frac{\Omega_S h^2}{\Omega_{Pl} h^2} = \frac{Y_{S,\infty} \cdot m_S}{T_{\rm eq}} \simeq 150\sqrt{10}\pi^2 \sqrt{\frac{g_*(T_{\rm fo})}{g_{*S}^2(T_{\rm fo})}} \frac{1}{M_{\rm Pl} T_{\rm eq}} \frac{m_S^2}{|\lambda_{HS}|^2} \left(1 - \frac{m_h^2}{m_S^2}\right)^{-1/2} , \tag{B.18}$$

where $g_*(T_{\rm fo}) \simeq 106.75$, $g_{*S}(T_{\rm fo}) \simeq 106.3$, $T_{\rm eq} = 0.4 \times 10^{-9}$ GeV and $M_{\rm Pl} \simeq 1.22 \times 10^{19}$ GeV. Therefore, by fixing the ratio f_S to a given value, the parameter space for the combination of values of λ_{HS} and m_S can be determinated, an analysis done in Section 6.

C Cosmological constraints on $\Delta N_{\rm eff}$

In this section we are interested on computing the effect of the extra electromagnetic injection, produced in the decay $S \to \chi\nu$, on the effective number of relativistic species $N_{\rm eff}$. To do so, we must quantify the effect of the neutrinos, which is encoded in the parameter

$$\Delta N_{\rm eff} = \frac{8}{7}\left(\frac{11}{4}\right)^{4/3} \left(\frac{\rho_{\rm dark}}{\rho_\gamma}\right) , \tag{C.1}$$

where the dark energy density is defined as $\rho_{\rm dark} = E_\nu(T_{\rm CMB}) n_{\nu_{\rm CMB}}$, with the number density $n_{\nu_{\rm CMB}} = Y_S \; s(T_{\rm CMB})$. The energy at the CMB is given by the redshifted energy at the decay,

$$E_\nu(T_{\rm CMB}) = \frac{T_{\rm CMB}}{T_{\rm dec}} E_\nu(T_{\rm dec}), \quad \text{where} \quad E_\nu(T_{\rm dec}) = \frac{m_S}{2}\left(1 - \frac{m_\chi^2}{m_S^2}\right) . \tag{C.2}$$

When it comes to the energy density of the photons, for a relativistic specie in equilibrium with the thermal bath, it is defined as

$$\rho_\gamma = g_\gamma \int \frac{d^3p}{(2\pi)^3} E(p) f(p) = \frac{\pi^2}{15} T^4 , \tag{C.3}$$

where it has been used the internal degrees of freedom $g_\gamma = 2$, and the definitions for massless photons $E(p) = p$ and $f(p) = 1/e^{p/T} - 1$ (Bose-Einstein distribution). Finally, using the definitions of the entropy and the temperature at the decay given by Eq. 5.13 and 5.22, it is possible to relate $\Delta N_{\rm eff}$ with the lifetime as

$$\Delta N_{\rm eff} \simeq \frac{8}{21}\left(\frac{11}{4}\right)^{4/3} \left(\frac{1.66\sqrt{g_*(T_{\rm dec})}}{M_{\rm Pl}}\right)^{1/2} g_{*S}(T_{\rm CMB}) T_{\rm eq} \left(1 - \frac{m_\chi^2}{m_S^2}\right) f_S \sqrt{\tau_S} , \tag{C.4}$$

where it has been used that $f_S \; T_{\rm eq} = m_S \; Y_S$. The importance of this expression lies in the fact that it connects the observable effects on $\Delta N_{\rm eff}$ with the abundance and lifetime of the dark scalar S, thereby allowing one to establish a set of constraints that reduce the viable parameter space of τ_S and m_S.

References

[1] Juan Herrero-Garcia, Giacomo Landini, and Tsutomu T. Yanagida. "Dark matter in the high-scale seesaw leptogenesis paradigm". In: Phys. Rev. D 111.7 (2025), p. 075033. DOI: 10.1103/PhysRevD.111.075033. arXiv: 2411.03452 [hep-ph].

[2] Wolfgang Pauli. Letter to the Physical Society of Tübingen. Unpublished letter, December 4, 1930. 1930.

[3] C. L. Cowan Jr. et al. "Detection of the Free Neutrino: a Confirmation". In: Science 124.3212 (July 1956), pp. 103–104. DOI: 10.1126/science.124.3212.103.

[4] Alessandro Granelli. "Standard and Non-Standard Aspects of Neutrino Physics". In: Universe 10.4 (2024), p. 164. DOI: 10.3390/universe10040164. arXiv: 2403.16308 [hep-ph].

[5] Peter Minkowski. "$\mu \to e\gamma$ at a Rate of One Out of 10^9 Muon Decays?" In: Phys. Lett. B 67 (1977), pp. 421–428. DOI: 10.1016/0370-2693(77)90435-X.

[6] Sacha Davidson, Enrico Nardi, and Yosef Nir. "Leptogenesis". In: Phys. Rept. 466 (2008), pp. 105–177. DOI: 10.1016/j.physrep.2008.06.002. arXiv: 0802.2962 [hep-ph].

[7] Sacha Davidson. "Neutrinos in cosmology". In: AIP Conf. Proc. 981.1 (2008). Ed. by Osamu Yasuda, Naba Mondal, and Chihiro. Ohmori, pp. 70–74. DOI: 10.1063/1.2899004.

[8] Chee Sheng Fong, Enrico Nardi, and Antonio Riotto. "Leptogenesis in the Universe". In: Adv. High Energy Phys. 2012 (2012), p. 158303. DOI: 10.1155/2012/158303. arXiv: 1301.3062 [hep-ph].

[9] W. Buchmuller. "Neutrinos in the early universe". In: Comptes Rendus Physique 6 (2005), pp. 798–809. DOI: 10.1016/j.crhy.2005.07.007.

[10] Richard H. Cyburt, Brian D. Fields, and Keith A. Olive. "Primordial Nucleosynthesis in Light of WMAP". In: Phys. Lett. B 567.3-4 (2003), pp. 227–234. DOI: 10.1016/j.physletb.2003.06.026. arXiv: astro-ph/0302431 [astro-ph].

[11] M. Fukugita and T. Yanagida. "Baryogenesis Without Grand Unification". In: Phys. Lett. B 174 (1986), pp. 45–47. DOI: 10.1016/0370-2693(86)91126-3.

[12] W. Buchmuller, R. D. Peccei, and T. Yanagida. "Leptogenesis as the origin of matter". In: Ann. Rev. Nucl. Part. Sci. 55 (2005), pp. 311–355. DOI: 10.1146/annurev.nucl.55.090704.151558. arXiv: hep-ph/0502169.

[13] W. Buchmüller. "Baryon asymmetry and thermal leptogenesis". In: Nucl. Phys. B Proc. Suppl. 143 (2005). Ed. by J. Dumarchez, F. Vannucci, and T. Patzak, pp. 462–469. DOI: 10.1016/j.nuclphysbps.2005.01.145.

[14] Dietrich Bodeker and Wilfried Buchmuller. "Baryogenesis from the weak scale to the grand unification scale". In: Rev. Mod. Phys. 93.3 (2021), p. 035004. DOI: 10.1103/RevModPhys.93.035004. arXiv: 2009.07294 [hep-ph].

[15] Alessandro Strumia. "Baryogenesis via leptogenesis". In: Les Houches Summer School on Theoretical Physics. Aug. 2006, pp. 655–680. arXiv: hep-ph/0608347.

[16] Particle Data Group et al. "Review of Particle Physics". In: Progress of Theoretical and Experimental Physics 2022.8 (Aug. 2022), p. 083C01. ISSN: 2050-3911. DOI: 10.1093/ptep/ptac097. eprint: https://academic.oup.com/ptep/article-pdf/2022/8/083C01/49175539/ptac097.pdf. URL: https://doi.org/10.1093/ptep/ptac097.

[17] Y. Fukuda et al. "Evidence for Oscillation of Atmospheric Neutrinos". In: Physical Review Letters 81.8 (1998), pp. 1562–1567. DOI: 10.1103/PhysRevLett.81.1562.

[18] B. Pontecorvo. "Inverse beta processes and nonconservation of lepton charge". In: Zh. Eksp. Teor. Fiz. 34 (1958). In Russian; cited as 1957 due to submission year, p. 247.

[19] B. Pontecorvo. "Mesonium and antimesonium". In: Sov. Phys. JETP 6 (1957). Original: Zh. Eksp. Teor. Fiz. 33 (1957) 549, pp. 429–431.

[20] Z. Maki, M. Nakagawa, and S. Sakata. "Remarks on the Unified Model of Elementary Particles". In: Progress of Theoretical Physics 28.5 (1962), pp. 870–880. DOI: 10.1143/PTP.28.870.

[21] K. A. Olive et al. "Review of Particle Physics". In: Chinese Physics C 38.9 (2014), p. 090001. DOI: 10.1088/1674-1137/38/9/090001.

[22] I. Esteban et al. "The fate of hints: Updated global analysis of three-flavor neutrino oscillations". In: Journal of High Energy Physics 2020.9 (2020), p. 178. DOI: 10.1007/JHEP09(2020)178.

[23] F. Capozzi et al. "Unfinished fabric of the three neutrino paradigm". In: Physical Review D 104.8 (2021), p. 083031. DOI: 10.1103/PhysRevD.104.083031.

[24] NuFIT Collaboration. NuFIT v5.2. http://www.nu-fit.org. Accessed on 28 March 2024. 2024.

[25] A. D. Sakharov. "Violation of CP Invariance, C Asymmetry, and Baryon Asymmetry of the Universe". In: JETP Letters 5 (1967). Pisma Zh. Eksp. Teor. Fiz. 5 (1967) 32, pp. 24–27.

[26] A. Riotto and M. Trodden. "Recent Progress in Baryogenesis". In: Annual Review of Nuclear and Particle Science 49 (1999), pp. 35–75. DOI: 10.1146/annurev.nucl.49.1.35.

[27] Edward W. Kolb and Michael S. Turner. The Early Universe. Vol. 69. Taylor and Francis, May 2019. ISBN: 978-0-429-49286-0, 978-0-201-62674-2. DOI: 10.1201/9780429492860.

[28] Planck Collaboration, P. A. R. Ade, et al. "Planck 2013 results. XXII. Constraints on inflation". In: Astronomy & Astrophysics 571 (2014), A22. DOI: 10.1051/0004-6361/201321569.

[29] Planck Collaboration, Y. Akrami, et al. "Planck 2018 results. X. Constraints on inflation". In: Astronomy & Astrophysics 641 (2020), A10. DOI: 10.1051/0004-6361/201833887.

[30] C. L. Bennett et al. "First-Year Wilkinson Microwave Anisotropy Probe (WMAP) Observations: Preliminary Maps and Basic Results". In: Astrophysical Journal Supplement Series 148 (2003), pp. 1–27. DOI: 10.1086/377253.

[31] Planck Collaboration. "Planck 2018 Results. VI. Cosmological Parameters". In: Astron. Astrophys. 641 (2020), A6. DOI: 10.1051/0004-6361/201833910.

[32] W. M. Yao et al. "Review on Big-Bang Nucleosynthesis in Review of Particle Physics". In: Journal of Physics G: Nuclear and Particle Physics 33 (2006), pp. 1–1232. DOI: 10.1088/0954-3899/33/1/001.

[33] J. Dunkley et al. "Five-Year Wilkinson Microwave Anisotropy Probe (WMAP) Observations: Likelihoods and Parameters from the WMAP data". In: The Astrophysical Journal Supplement Series 180.2 (2009), pp. 306–329. DOI: 10.1088/0067-0049/180/2/306. eprint: arXiv:0803.0586.

[34] N. S. Manton. "Topology in the Weinberg-Salam Theory". In: Physical Review D 28 (1983), pp. 2019–2026. DOI: 10.1103/PhysRevD.28.2019.

[35] F. R. Klinkhamer and N. S. Manton. "A saddle-point solution in the Weinberg-Salam theory". In: Physical Review D 30 (1984), pp. 2212–2220. DOI: 10.1103/PhysRevD.30.2212.

[36] Vera C. Rubin and W. Kent Ford Jr. "Rotation of the Andromeda Nebula from a Spectroscopic Survey of Emission Regions". In: Astrophys. J. 159 (1970), pp. 379–403. DOI: 10.1086/150317.

[37] Planck Collaboration, Y. Akrami, et al. "Planck 2018 results. VI. Cosmological parameters". In: Astronomy & Astrophysics 641 (2020), A6. DOI: 10.1051/0004-6361/201833910.

[38] Planck Collaboration. "Planck 2018 results. VI. Cosmological parameters". In: Astronomy & Astrophysics 641 (2020), A6. DOI: 10.1051/0004-6361/201833910. eprint: arXiv:1807.06209.

[39] Marco Cirelli, Alessandro Strumia, and Jure Zupan. "Dark Matter". In: (June 2024). arXiv: 2406.01705 [hep-ph].

[40] Julia Garayoa, María C. González-García, and Nuria Rius. "Soft leptogenesis in the inverse seesaw model". In: Journal of High Energy Physics 2007.02 (2007), p. 021. DOI: 10.1088/1126-6708/2007/02/021. arXiv: hep-ph/0611311 [hep-ph].

[41] J. Racker, Manuel Peña, and Nuria Rius. "Leptogenesis with small violation of B − L". In: JCAP 2012.07 (2012), p. 030. DOI: 10.1088/1475-7516/2012/07/030. arXiv: 1205.1948 [hep-ph].

[42] Mayumi Aoki, Naoyuki Haba, and Ryo Takahashi. "A model realizing inverse seesaw and resonant leptogenesis". In: Prog. Theor. Exp. Phys. 11 (2015), 113B03. DOI: 10.1093/ptep/ptv149. arXiv: 1506.06946 [hep-ph].

[43] Juraj Klarić, Mikhail Shaposhnikov, and Inar Timiryasov. "Uniting Low-Scale Leptogenesis Mechanisms". In: Phys. Rev. Lett. 127.11 (2021), p. 111802. DOI: 10.1103/PhysRevLett.127.111802. arXiv: 2008.13771 [hep-ph].

[44] Juraj Klarić, Mikhail Shaposhnikov, and Inar Timiryasov. "Reconciling resonant leptogenesis and baryogenesis via neutrino oscillations". In: Phys. Rev. D 104.5 (2021), p. 055010. DOI: 10.1103/PhysRevD.104.055010. arXiv: 2103.16545 [hep-ph].

[45] Marco Drewes, Yannis Georis, and Juraj Klarić. "Mapping the Viable Parameter Space for Testable Leptogenesis". In: Phys. Rev. Lett. 128.5 (2022), p. 051801. DOI: 10.1103/PhysRevLett.128.051801. arXiv: 2106.16226 [hep-ph].

[46] Marco Drewes et al. "Low-scale leptogenesis with flavour and CP symmetries". In: JHEP 12 (2022), p. 044. DOI: 10.1007/JHEP12(2022)044. arXiv: 2203.08538 [hep-ph].

[47] A. M. Sirunyan *et al.* "Search for long-lived particles using displaced vertices and missing transverse momentum in proton–proton collisions at $\sqrt{s} = 13$ TeV". In: Journal of High Energy Physics 07 (2020), p. 122. DOI: 10.1007/JHEP07(2020)122. arXiv: 2001.11522 [hep-ex].

[48] Joscha Knolle. "Prompt searches for feebly interacting particles at the LHC". In: PoS LHCP2024 (2025), p. 180. DOI: 10.22323/1.478.0180. arXiv: 2412.06297 [hep-ex].

[49] Xiaocong Ai et al. "Flavor Physics at CEPC: a General Perspective". In: (Dec. 2024). arXiv: 2412.19743 [hep-ex].

[50] Martin Aleksa. FCC-hh – Physics Requirements and Reference Detector. Conference presentation slides. Oct. 2, 2024. URL: https://agenda.infn.it/event/42594/contributions/242609/attachments/126368/186542/Hadron-Collider-WS-20241002.pdf (visited on 07/03/2025).

[51] Luis A. Anchordoqui et al. "The Forward Physics Facility: Sites, Experiments, and Physics Potential". In: Physics Reports 968 (2022), pp. 1–50. DOI: 10.1016/j.physrep.2022.04.004. arXiv: 2109.10905 [hep-ph].

[52] SHiP Collaboration. Search for Hidden Particles at the High-Intensity ECN3 Facility. https://ship.web.cern.ch/. Website, accessed 7 July 2025. CERN, 2025.

[53] Georges Lemaître. "Un univers homogène de masse constante et de rayon croissant, rendant compte de la vitesse radiale des nébuleuses extragalactiques". fr. In: Annales de la Société Scientifique de Bruxelles A47 (1927). First proposal of an expanding universe model, pp. 49–59.

[54] Albert Einstein. "Die Feldgleichungen der Gravitation". de. In: Sitzungsberichte der Preussischen Akademie der Wissenschaften zu Berlin (1915). Presentation of the field equations of general relativity, pp. 844–847.

[55] Lawrence J. Hall et al. "Freeze-In Production of FIMP Dark Matter". In: JHEP 03 (2010), p. 080. DOI: 10.1007/JHEP03(2010)080. arXiv: 0911.1120 [hep-ph].

[56] Sacha Davidson and Alejandro Ibarra. "A Lower bound on the right-handed neutrino mass from leptogenesis". In: Phys. Lett. B 535 (2002), pp. 25–32. DOI: 10.1016/S0370-2693(02)01735-5. arXiv: hep-ph/0202239.

[57] A. Abada et al. "Flavour Matters in Leptogenesis". In: JHEP 09 (2006), p. 010. DOI: 10.1088/1126-6708/2006/09/010. arXiv: hep-ph/0605281.

[58] Scott Dodelson and Lawrence M. Widrow. "Sterile-neutrinos as dark matter". In: Phys. Rev. Lett. 72 (1994), pp. 17–20. DOI: 10.1103/PhysRevLett.72.17. arXiv: hep-ph/9303287.

[59] Xun Shi and George M. Fuller. "A New dark matter candidate: Nonthermal sterile neutrinos". In: Phys. Rev. Lett. 82 (1999), pp. 2832–2835. DOI: 10.1103/PhysRevLett.82.2832. arXiv: astro-ph/9810076.

[60] Shao-Ping Li and Xun-Jie Xu. "Dark matter produced from right-handed neutrinos". In: arXiv preprint (Dec. 2022). Preprint, doi:10.48550/arXiv.2212.09109. arXiv: 2212.09109 [hep-ph].

[61] Adam Falkowski et al. "Light dark matter from leptogenesis". In: Phys. Rev. D 99 (1 Jan. 2019), p. 015022. DOI: 10.1103/PhysRevD.99.015022. URL: https://link.aps.org/doi/10.1103/PhysRevD.99.015022.

[62] Adam Falkowski, Joshua T. Ruderman, and Tomer Volansky. "Asymmetric Dark Matter from Leptogenesis". In: Journal of High Energy Physics 2011.5 (May 2011), p. 106. DOI: 10.1007/JHEP05(2011)106. arXiv: 1101.4936 [hep-ph].

[63] Lawrence J. Hall et al. "Freeze-in production of FIMP dark matter". In: Journal of High Energy Physics 2010.3 (Mar. 2010), p. 080. DOI: 10.1007/JHEP03(2010)080. arXiv: 0911.1120 [hep-ph].

[64] ATLAS Collaboration. "Combined measurement of the Higgs boson mass in the diphoton and four-lepton decay channels using pp collision data at $\sqrt{s} = 13$TeV with the ATLAS detector". In: Phys. Lett. B 833 (2022), p. 137379. DOI: 10.1016/j.physletb.2022.137379.

[65] Oleg Lebedev. "The Higgs portal to cosmology". In: Prog. Part. Nucl. Phys. 120 (2021), p. 103881. DOI: 10.1016/j.ppnp.2021.103881. arXiv: 2104.03342 [hep-ph].

[66] Alexey Boyarsky et al. "When feebly interacting massive particles decay into neutrinos: The Neff story". In: Phys. Rev. D 104.3 (2021), p. 035006. DOI: 10.1103/PhysRevD.104.035006. arXiv: 2103.09831 [hep-ph].

[67] Thomas Hambye, Marco Hufnagel, and Matteo Lucca. "Cosmological constraints on the decay of heavy relics into neutrinos". In: JCAP 05.05 (2022), p. 033. DOI: 10.1088/1475-7516/2022/05/033. arXiv: 2112.09137 [hep-ph].

[68] Sara Bianco et al. "Photo- and Hadrodisintegration constraints on massive relics decaying into neutrinos". In: (May 2025). arXiv: 2505.01492 [hep-ph].

[69] Nils Schöneberg. "The 2024 BBN baryon abundance update". In: JCAP 06.006 (2024). DOI: 10.1088/1475-7516/2024/06/006. arXiv: 2401.15054 [astro-ph.CO].

[70] P. A. Zyla et al. "Review of Particle Physics". In: Prog. Theor. Exp. Phys. 2020.8 (Aug. 2020). Published by Progress of Theoretical and Experimental Physics, Issue 08, 15 Aug 2020, p. 083C01. DOI: 10.1093/ptep/ptaa104. URL: https://academic.oup.com/ptep/article/2020/8/083C01/5891211.

[71] Planck Collaboration et al. "Planck 2018 results. VI. Cosmological parameters". In: Astron. Astrophys. 641 (2020). Erratum: Astron. Astrophys. 652, C4 (2021), A6. DOI: 10.1051/0004-6361/201833910. arXiv: 1807.06209 [astro-ph.CO].

[72] CMB-S4 Collaboration et al. CMB-S4 Science Book, First Edition. Technical Report 1610.02743. First Edition, arXiv:1610.02743 [astro-ph.CO]. arXiv, 2016.

[73] Kevork N. Abazajian et al. "CMB-S4 Science Case, Reference Design, and Project Plan". In: arXiv e-prints 1907.04473 (2019). Preprint; not peer-reviewed. arXiv: 1907.04473 [astro-ph.IM].

[74] Simone Aiola and CMB-HD Collaboration. "Snowmass2021 CMB-HD White Paper". In: (2022). CMB-HD Collaboration white paper for Snowmass 2021. arXiv: 2203.05728 [astro-ph.CO].

[75] Vid Iršič et al. "New Constraints on the free-streaming of warm dark matter from intermediate and small scale Lyman- forest data". In: Physical Review D 96.2 (2017), p. 023522. DOI: 10.1103/PhysRevD.96.023522. arXiv: 1702.01764 [astro-ph.CO].

[76] A. Boyarsky et al. "Lyman-alpha constraints on warm and on warm-plus-cold dark matter models". In: Journal of Cosmology and Astroparticle Physics 2009.05 (2009), p. 012. DOI: 10.1088/1475-7516/2009/05/012. arXiv: 0812.0010 [astro-ph].

[77] Q. Decant et al. "Lyman- constraints on freeze-in and superWIMPs". In: Journal of Cosmology and Astrophyisics 2022.03 (2022), p. 041. DOI: 10.1088/1475-7516/2022/03/041. arXiv: 2111.09321 [astro-ph.CO].

[78] James M. Cline et al. "Update on scalar singlet dark matter". In: Physical Review D 88.5 (2013), p. 055025. DOI: 10.1103/PhysRevD.88.055025. arXiv: 1306.4710 [hep-ph].

[79] M. Aker et al. "Direct neutrino-mass measurement based on 259 days of KATRIN data". In: Science 388.6743 (2025), pp. 180–185. DOI: 10.1126/science.adq9592.

[80] Ludwig Boltzmann. "Weitere Studien über das Wärmegleichgewicht unter Gasmolekülen". In: Wiener Berichte 66 (1872), pp. 275–370.

[81] Paolo Gondolo and Graciela Gelmini. "Cosmic abundances of stable particles: Improved analysis". In: Nucl. Phys. B 360 (1991), pp. 145–179. DOI: 10.1016/0550-3213(91)90438-4.